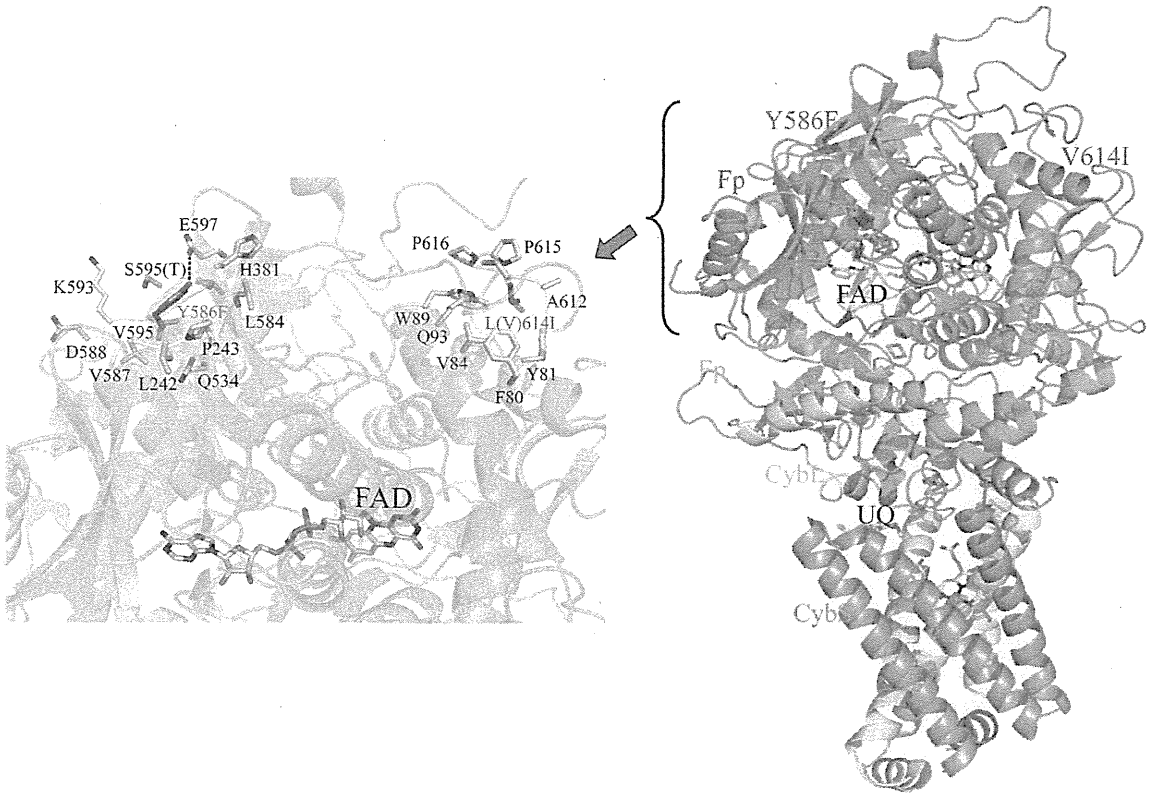

Fig. 7. Positions of Tyr 586 and Val 614 in the structure of porcine complex II. The two amino acid residues that are different in human isoforms, Y586F and V614I, are shown in a cartoon representation of the porcine complex II structure (right) and a close-up view of the region including Y586F and V614I (left). V614I is surrounded mainly by hydrophobic residues, whereas Y586F is surrounded by both hydrophilic and hydrophobic residues. Y586 and E597 are within the hydrogen bond distance (3.15 Å) to each other. UQ shows ubiquinone. The numbers of the amino acid residues indicate the human amino acid sequence. The amino acids in parentheses show the human amino acids that are different from the porcine amino acids. Modified image from Sakai et al. (2012).

Embryogenesis occurs in a hypoxic environment until 8–12 weeks (Kingdom and Kaufmann, 1999), and organogenesis of the kidney, lung and cardiovascular system occurs in a low-oxygen environment (McGovern et al., 2010). Some cancer tissues are in a hypoxic environment or poor nutrition conditions (Izuishi et al., 2000). In addition, a couple of fetal tissues and cancer tissues predominantly express type II Fp (Sakai et al., 2012; Tomitsuka et al., 2003a,b). Thus, type II Fp may play an important role in fetal development and cancer tissue metabolism.

Recently, we showed that cancer cells utilize fumarate respiration under hypoxia or poor nutrition conditions (Tomitsuka et al., 2009, 2011, 2012). Fumarate respiration is a well-known electron transport chain found in anaerobic bacteria (Kita et al., 2007; Kroger et al., 1992) and parasitic helminthes such as *Ascaris suum* (Harada et al., 2013; Sakai et al., 2012). The reducing equivalent of NADH is transferred to low-potential quinone such as rhodoquinone by complex I and finally is oxidized by the quinol-fumarate reductase (QFR) activity of complex II, which is a reverse reaction of the SQR activity of complex II. By using this respiratory chain, the parasites are able to synthesize ATP even in the absence of oxygen. We previously showed that *A. suum* mitochondria express stage-specific isoforms of Fp and the CybS subunit; two distinct complex IIs function as SQR in larvae or QFR in adults (Amino et al., 2000; Kita et al., 2002; Kuramochi et al., 1994; Saruta et al., 1996). On the other hand, only one peptide is found for each subunit of human complex II except Fp.

There remains a question on which complex II is responsible for fumarate respiration in human cancer cells. In this study, we show that complex II^{II} is important for cells under hypoxia or poor nutrition which is similar to the condition of cancer cells. In this regard, complex II^{II} could be one of the candidates which play an important role in fumarate respiration in human mitochondria as the terminal oxidase of the system. Crystal structure analysis showed that the structure of *A. suum* adult QFR is more closely related to mammalian SQR than bacterial QFR (Shimizu et al., 2012), indicating that mitochondrial SQR-type complex II is able to catalyze QFR activity. In addition, our latest study on the mechanism of fumarate reduction by *A. suum* QFR using 3D structure of the enzyme revealed that a partial charge separation and the twisted conformation of fumarate are the key to the reduction of fumarate (Harada et al., 2013). Expression of two types of human complex II for crystal structure analysis is now in progress.

5. Conclusion

In this study, we clearly showed that complex II with type I Fp mainly functions as SQR in human mitochondria under normal conditions and that complex II with type II Fp may play an important role for adaptation to hypoxia and nutrition-deprived conditions, especially in tumor and fetal tissues. To understand the role of type II Fp in more detail, biochemical properties of complex IIs with each isoform should be further investigated.

Acknowledgments

This work was supported in part by Creative Scientific Research Grant 18GS0314 (to KK), Grant-in-aid for Scientific Research on Priority Areas 18073004 (to KK) from the Japanese Society for the Promotion of Science, Targeted Proteins Research Program (to KK) from the Japanese

Ministry of Education, Science, Culture, Sports and Technology (MEXT) and by a grant to KK and SH from the Program for Promotion of Basic and Applied Researches for Innovations in Bio-oriented Industry (BRAIN).

References

Ackrell, B.A., Kearney, E.B., Mayr, M., 1974. Role of oxalacetate in the regulation of mammalian succinate dehydrogenase. J. Biol. Chem. 249, 2021–2027.

Amino, H., Wang, H., Hirawake, H., Saruta, F., Mizuchi, D., Mineki, R., Shindo, N., Murayama, K., Takamiya, S., Aoki, T., Kojima, S., Kita, K., 2000. Stage-specific isoforms of *Ascaris suum* complex II: the fuma rate reductase of the parasitic adult and the succinate dehydrogenase of free-living larvae share a common iron-sulfur subunit. Mol. Biochem. Parasitol. 106, 63–76.

Balut, C., vandeVen, M., Despa, S., Lambrichts, I., Ameloot, M., Steels, P., Smets, I., 2008. Measurement of cytosolic and mitochondrial pH in living cells during reversible metabolic inhibition. Kidney Int. 73, 226–232.

Baron, S., Caplanusi, A., van de Ven, Martin, Radu, M., Despa, S., Lambrichts, S., Ameloot, M., Steels, P., Smets, I., 2005. Role of mitochondrial Na^+ concentration, measured by CoroNa Red, in the protection of metabolically inhibited MDCK cells. J. Am. Soc. Nephrol. 16, 3490–3497.

Bayley, J.P., Devilee, P., Taschner, E.M.P., 2005. The SDH mutation database: an online resource for succinate dehydrogenase sequence variants involved in pheochromocytoma, paraganglioma and mitochondrial complex II deficiency. BMC Med. Genet. 6, 391.

Baysal, B.E., 2003. On the association of succinate dehydrogenase mutations with hereditary paraganglioma. Trends Endocrinol. Metab. 14, 453–459.

Baysal, B.E., Lawrence, E.C., Ferrell, R.E., 2007. Sequence variation in human succinate dehydrogenase genes: evidence for long-term balancing selection on SDHA. BMC Biol. 5, 12.

Bourgeron, T., Rustin, P., Chretien, D., Birch-Machin, M., Bourgeois, M., Viegas-Pequignot, E., Munnich, A., Rotig, A., 1995. Mutation of a nuclear succinate dehydrogenase gene results in mitochondrial respiratory chain deficiency. Nat. Genet. 11, 144–149.

Briere, J.J., Favier, J., Benit, P., Ghouzzi, V., Lorenzato, A., Rabier, D., Flavia, M., Gimenez-Roqueplo, A.P., Rustin, P., 2005. Mitochondrial succinate is instrumental for HIF1*a* nuclear translocation in SDHA-mutant fibroblasts under normoxic conditions. Hum. Mol. Genet. 14, 3263–3269.

Brockmann, K., Bjornstad, A., Dechent, P., Korenke, C.G., Smeitink, J., Frans Trijbels, J.M., Athanassopoulos, S., Villagran, R., Skjeldal, O.H., Wilichowski, E., Frahm, J., Hanefeld, F., 2002. Succinate in dystrophic white matter: a proton magnetic resonance spectroscopy finding characteristic for complex II deficiency. Ann. Neurol. 52, 38–46.

Burnichon, N., Brière, J.J., Libe, R., Vescovo, L., Riviere, J., Tissier, F., Jouanno, E., Jeunemaitre, X., Benit, P., Tzagoloff, A., Rustin, P., Bertherat, J., Favier, J., Gimenez-Roqueplo, A.P., 2010. SDHA is a tumor suppressor gene causing paraganglioma. Hum. Mol. Genet. 19, 3011–3020.

Busch, H., Potter, V.R., 1952. Succinate accumulation *in vivo* following injection of malonate. J. Biol. Chem. 198, 71–77.

Caplanusi, A., Fuller, A.J., Villalobos, G., Hammond, T.G., Navar, L.G., 2007. Metabolic inhibition-induced transient Ca^{2+} increase depends on mitochondria in a human proximal renal cell line. Am. J. Physiol. Renal Physiol. 293, 533–540.

Eng, C., Kiuru, M., Fernandez, M.J., Aaltonen, L.A., 2003. A role for hypoxic mitochondrial enzymes in inherited neoplasia and beyond. Nat. Rev. Cancer 3, 193–202.

Ghezzi, D., Goffrini, P., Uziel, G., Horvath, R., Klopstock, T., Lochmüller, H., D'Adamo, P., Gasparini, P., Strom, T.M., Prokisch, H., Invernizzi, F., Ferrero, I., Zeviani, M., 2009. SDHAF1, encoding a LYR complex-II specific assembly factor, is mutated in SDH-defective infantile leukoencephalopathy. Nat. Genet. 41, 654–656.

Hao, H.X., Khalimonchuk, O., Schraders, M., Dephoure, N., Bayley, J.P., Kunst, H., Devilee, P., Cremers, C.W., Schiffman, J.D., Bentz, B.G., Gygi, S.P., Winge, D.R., Kremer, H., Rutter, J., 2009. SDH5, a gene required for flavination of succinate dehydrogenase, is mutated in paraganglioma. Science 325, 1139–1142.

Harada, S., Inaoka, D.K., Ohmori, J., Kita, K., 2013. Diversity of parasite complex II. Biochim. Biophys. Acta 1827, 658–667.

Huang, L.S., Sun, G., Cobessi, D., Wang, A.C., Shen, J.T., Tung, E.Y., Anderson, V.E., Berry, E.A., 2006. 3-nitropropionic acid is a suicide inhibitor of mitochondrial respiration that, upon oxidation by complex II, forms a covalent adduct with a catalytic base arginine in the active site of the enzyme. J. Biol. Chem. 281 (9), 5965–5972.

Ishii, N., Ishii, T., Hartman, P.S., 2007. The role of the electron transport SDHC gene on lifespan and cancer. Mitochondrion 7, 24–38.

Iverson, T.M., Maklashina, E., Cecchini, G., 2012. Structural basis for malfunction in complex II. J. Biol. Chem. 287, 35430–35438.

Izuishi, K., Kato, K., Ogura, T., Kinoshita, T., Esumi, H., 2000. Remarkable tolerance of tumor cells to nutrient deprivation: possible new biochemical target for cancer therapy. Cancer Res. 60, 6201–6207.

Killian, J.K., Kim, S.Y., Miettinen, M., et al., 2013. Succinate dehydrogenase mutation underlies global epigenomic divergence in gastrointestinal stromal tumor. Cancer Discov. 10, 2159–8290.

Kingdom, J.C., Kaufmann, P., 1999. Oxygen and placental vascular development. Adv. Exp. Med. Biol. 474, 259–275.

Kita, K., Hirawake, H., Miyadera, H., Amino, H., Takeo, S., 2002. Role of complex II in anaerobic respiration of the parasite mitochondria from *Ascaris suum* and *Plasmodium falciparum*. Biochem. Biophys. Acta 1553, 123–139.

Kita, K., Shiomi, K., Ōmura, S., 2007. Parasitology in Japan: advances in drug discovery and biochemical studies. Trends Parasitol. 23, 223–229.

Kler, R.S., Jackson, S., Bartkett, K., Bindoff, L.A., Eaton, S., Pourfarzan, M., Frerman, F.E., Gooldman, S.I., Watmough, N.J., Turnbull, D.M., 1991. Quantitation of Acyl-CoA and Acylcarnitine esters accumulated during abnormal mitochondria fatty acid oxidation. J. Biol. Chem. 266, 22932–22938.

Kroger, A., Geisler, V., Lemma, E., Theis, F., Lenger, R., 1992. Bacterial fumarate respiration. Arch. Microbiol. 158, 311–314.

Kuramochi, T., Hirawake, H., Kojima, S., Takamiya, S., Furushima, R., Aoki, T., Komuniecki, R., Kita, K., 1994. Sequence comparison between the flavoprotein subunit of the fumarate reductase (complex II) of the anaerobic parasitic nematode, *Ascaris suum* and the succinate dehydrogenase of theaerobic, free-living nematode, *Caenorhabditis elegans*. Mol. Biochem. Parasitol. 68, 177–187.

Llopis, J., McCaffery, J.M., Miyawaki, A., Farquhar, M.G., Tsien, R.Y., 1998. Measurement of cytosolic, mitochondrial, and Golgi pH in single living cells with green fluorescent proteins. \Proc. Natl. Acad. Sci. U. S. A. 95, 6803–6808.

McGovern, S., Pan, J., Oliver, G., Cutz, E., Yeger, H., 2010. The role of hypoxia and neurogenic genes (Mash-1 and Prox-1) in the developmental programming and maturation of pulmonary neuroendocrine cells in fetal mouse lung. Lab. Invest. 90, 180–195.

Miyadera, H., Shiomi, K., Ui, H., Yamaguchi, Y., Masuma, R., Tomoda, H., Miyoshi, H., Osanai, A., Kita, K., Ōmura, S., 2003. Atpenins, potent and specific inhibitors of mitochondrial complex II (succinate-ubiquinone oxidoreductase). Proc. Natl. Acad. Sci. U. S. A. 100, 473–477.

Miyagishi, M., Taira, K., 2002. U6 promoter-driven siRNAs with four uridine 3' overhangs efficiently suppress targeted gene expression in mammalian cells. Nat. Biotechnol. 20, 497–500.

Parfait, B., Chretien, D., Rötig, A., Marsac, C., Munnich, A., Rustin, P., 2000. Compound heterozygous mutations in the flavoprotein gene of the respiratory chain complex II in a patient with Leigh syndrome. Hum. Genet. 106, 236–243.

Pollard, P.J., Wortham, N.C., Tomlinson, I.P., 2003. The TCA cycle and tumorigenesis: the examples of fumarate hydratase and succinate dehydrogenase. Ann. Med. 35, 632–639.

Quinlan, C.L., Orr, A.L., Perevoshchikova, I.V., Treberg, J.R., Ackrell, B.A., Brand, M.D., 2012. Mitochondrial complex II can generate reactive oxygen species at high rates in both the forward and reverse reactions. J. Biol. Chem. 27255–27264.

Ramshesh, V.K., Lemasters, J.J., 2012. Imaging of mitochondrial pH using SNARF-1. Methods Mol. Biol. 810, 243–248.

Rustin, P., Rotig, A., 2002. Inborn errors of complex II–unusual human mitochondrial diseases. Biochim. Biophys. Acta 1553, 117–122.

Rutter, J., Winge, D.R., Schiffman, J.D., 2010. Succinate dehydrogenase – assembly, regulation and role in human disease. Mitochondrion 10, 393–401.

Sakai, C., Tomitsuka, E., Esumi, H., Harada, S., Kita, K., 2012. Mitochondrial fumarate reductase as a target of chemotherapy: from parasites to cancer cells. Biochim. Biophys. Acta 820, 643–651.

Salvi, M., Morrice, N., Brunati, A., Toninello, A., 2007. Identification of the flavoprotein of succinate dehydrogenase and aconitase as *in vitro* mitochondrial substrates of Fgr tyrosine kinase. FEBS Lett. 581, 5579–5585.

Saruta, F., Hirawake, H., Takamiya, S., Ma, Y.C., Aoki, T., Sekimizu, K., Kojima, S., Kita, K., 1996. Cloning of a cDNA encoding the small subunit of cytochrome b558 (cybS) of mitochondrial fumarate reductase (complex II) from adult *Ascaris suum*. Biochim. Biophys. Acta 1276, 1–5.

Schwarz, D.S., Ding, H., Kennington, L., Moore, J.T., Schelter, J., Burchard, J., Linsley, P.S., Aronin, N., Xu, Z., Zamore, P.D., 2006. Designing siRNA that distinguish between genes that differ by a single nucleotide. PLoS Genet. 2, e140.

Selak, M.A., Armour, S.M., MacKenzie, E.D., Boulahbel, H., Watson, D.G., Mansfield, K.D., Pan, Y., Simon, M.C., Thompson, C.B., Gottlieb, E., 2005. Succinate links TCA cycle dysfunction to oncogenesis by inhibiting HIF-alpha prolyl hydroxylase. Cancer Cell 7, 77–85.

Shimizu, H., Osanai, A., Sakamoto, K., Inaoka, D.K., Shiba, T., Harada, S., Kita, K., 2012. Crystal structure of mitochondrial quinol-fumarate reductase from the parasitic nematode *Ascaris suum*. J. Biochem. 151, 589–592.

Sun, F., Huo, X., Zhai, Y., Wang, A., Xu, J., Su, D., Bartlam, M., Rao, Z., 2005. Crystal structure of mitochondrial respiratory membrane protein complex II. Cell 121 (7), 1043–1057.

Takahashi, M., Watanabe, S., Murata, M., Furuya, H., Kanazawa, I., Wada, K., Hohjoh, H., 2010. Tailor-made RNAi knockdown against triplet repeat disease-causing alleles. Proc. Natl. Acad. Sci. U. S. A. 107, 21731–21736.

Toma, I., Kang, J.J., Sipos, A., Vargas, S., Bansal, E., Hanner, F., Meer, E., Peti-Peterdi, J., 2008. Succinate receptor GPR91 provides a direct link between high glucose levels and renin release in murine and rabbit kidney. J. Clin. Invest. 118, 2526–2534.

Tomitsuka, E., Hirawake, H., Goto, Y., Taniwaki, M., Harada, S., Kita, K., 2003a. Direct evidence for two distinct forms of the flavoprotein subunit of human mitochondrial complex II (succinate-ubiquinone reductase). J. Biochem. 134, 191–195.

Tomitsuka, E., Goto, Y., Taniwaki, M., Kita, K., 2003b. Direct evidence for expression of type II flavoprotein subunit in human complex II (succinate-ubiquinone reductase). Biochem. Biophys. Res. Commun. 311, 74–79.

Tomitsuka, E., Kita, K., Esumi, H., 2009. Regulation of succinate-ubiquinone reductase and fumarate reductase activities in human complex II by phosphorylation of its flavoprotein subunit. Proc. Jpn. Acad. Ser. B Phys. Biol. Sci. 85, 258–265.

Tomitsuka, E., Kita, K., Esumi, H., 2011. The NADH-fumarate reductase system, a novel mitochondrial energy metabolism, is a new target for anticancer therapy in tumor microenvironments. Ann. N. Y. Acad. Sci. 201, 44–49.

Tomitsuka, E., Kita, K., Esumi, H., 2012. An anticancer agent, pyrvinium pamonate inhibits the NADH-fumarate system—a unique mitochondrial energy metabolism in tumor microenvironments. J. Biochem. 52, 171–183.

Van Coster, R., Seneca, S., Smet, J., Van Hecke, R., Gerlo, E., Devreese, B., Van Beeumen, J., Leroy, J.G., De Meirleir, L., Lissens, W., 2003. Homozygous Gly555Glu mutation in the nuclear-encoded 70 kDa flavoprotein gene causes instability of the respiratory chain complex II. Am. J. Med. Genet. A 120, 13–18.

Wojtovich, A.P., Smith, C.O., Haynes, C.M., Nehrke, K.W., Brookes, P.S., 2013. Physiological consequences of complex II inhibition for aging, disease, and the mKATP channel. Biochim. Biophys. Acta 1827, 598–611.

Yu, D., Pendergraff, H., Liu, J., Kordasiewicz, H.B., Cleveland, D.W., Swayze, E.E., Lima, W.F., Crooke, S.T., Prakash, T.P., Corey, D.R., 2012. Single-stranded RNAs use RNAi to potently and allele-selectively inhibit mutant huntingtin expression. Cell 150, 895–908.

J. Biochem. 2013;154(6):501–504 doi:10.1093/jb/mvt096

JB THE JOURNAL OF BIOCHEMISTRY

Rapid communication

Synergy of ferrous ion on 5-aminolevulinic acid-mediated growth inhibition of *Plasmodium falciparum*

Received October 4, 2013; accepted October 18, 2013; published online October 24, 2013

Keisuke Komatsuya[1], Masayuki Hata[1], Emmanuel O. Balogun[1,2,3], Kenji Hikosaka[1], Shigeo Suzuki[1,4], Kiwamu Takahashi[4], Tohru Tanaka[4], Motowo Nakajima[4], Shun-Ichiro Ogura[5], Shigeharu Sato[6] and Kiyoshi Kita[1,*]

[1]Department of Biomedical Chemistry, Graduate School of Medicine, The University of Tokyo, 7-3-1 Hongo, Bunkyo-ku, Tokyo 113-0033; [2]Department of Applied Biology, Graduate School of Science and Technology, Kyoto Institute of Technology, Sakyo-ku, Kyoto 606-8585, Japan; [3]Department of Biochemistry, Ahmadu Bello University, Zaria 2222, Nigeria; [4]SBI Pharmaceuticals Co, LTD, Izumi Garden Tower 20F, 1-6-1, Roppongi, Minato-ku, Tokyo; [5]Graduate School of Bioscience and Biotechnology, Tokyo Institute of Technology, 4259-B102 Nagatsuta-cho, Midori-ku, Yokohama 226-8501, Japan; and [6]Division of Parasitology, MRC National Institute for Medical Research, The Ridgeway, Mill Hill, London NW7 1AA, UK

*Kiyoshi Kita, Department of Biomedical Chemistry, Graduate School of Medicine, University of Tokyo, 7-3-1 Hongo, Bunkyo-ku, Tokyo 113-0033, Japan. Tel: +81-3-5841-3526, Fax: +81-3-5841-3444, email: kitak@m.u-tokyo.ac.jp

Haem biosynthesis appeared to be a target of malaria therapy because 5-aminolevulinic acid (ALA), a haem biosynthesis starting material, with light exposure or a high amount of ALA alone reduced *Plasmodium falciparum* growth to undetectable level. However, the administration of a high dose of ALA is unrealistic for clinical therapy. We found that Fe^{2+} enhanced *P. falciparum*-killing potency of ALA and significantly inhibited the parasite growth. The intermediates of haem biosynthesis localized to the parasite organelles, and coproporphyrin III was the most accumulated intermediate. These novel findings may lead to development of a new anti-malarial drug using ALA and Fe^{2+}.

Keywords: 5-aminolevulinic acid (ALA)/Haem synthesis/malaria/*Plasmodium falciparum*.

Abbreviations: ACP, acyl carrier protein; ALA, 5-aminolevulinic acid; CPI, coproporphyrin I; CPIII, coproporphyrin III; FC, ferrochelatase; GFP, green fluorescent protein; PPIX, protoporphyrin IX; RBCs, red blood cells; ROS, reactive oxygen species; SFC, sodium ferrous citrate.

Malaria is a major global health problem, truncating over 1 million human lives annually, mainly children in the tropical and sub-tropical regions (*1*). The most lethal species of pathogens is *Plasmodium falciparum*, transmitted by the female *Anopheles* mosquitoes. They invade the hepatocytes first and differentiate into merozoites, which are released to infect red blood cells (RBCs) and establish the disease (*2*). The erythrocytic cycle is composed of the following stages: ring (early infection form), trophozoite (mature and undergo asexual division) and schizont (which ruptures RBCs and the resulting merozoites proceed to infect new RBCs).

Due to difficulties in anti-malarial vaccine development, it is pertinent to rely on chemotherapy to control malaria. However, the parasites are able to rapidly develop resistance against the available chemotherapies (*3*). Hence, new drugs with different modes of action are urgently needed. Enzymes in the pathways of macromolecular and metabolite biosynthesis such as haem production and degradation, have been recognized as novel chemotherapeutic targets in the *Plasmodium* (*4–9*).

Haem is an iron-containing complex macrocycle that plays a fundamental role in many cellular processes including oxygen transport (haemoglobin) and storage (myoglobin), mitochondrial electron transport complexes and detoxification (cytochrome) (*10*). Mitochondrion is an important organelle of the parasite, where Haem-containing proteins are necessary for its functions (*11*, *12*). Since atovaquone, an anti-malarial drug, specifically targets complex III (cytochrome bc_1) in *Plasmodium*, mitochondrial respiration must be fundamental for the parasite survival (*13*). Recent studies revealed that *Plasmodium* possesses *de novo* Haem synthesis and it plays an essential role in the mosquito and liver stages (*7*). Interestingly, the parasite does not salvage haem but rather polymerize Haems from host haemoglobin into haemozoin, as a mechanism of detoxification in its food vacuole to prevent production of reactive oxygen species (ROS) by free haem (*14*). This system is well known as the target of anti-malarial drug, chloroquine (*6*).

Generally in non-photosynthetic eukaryotes, haem biosynthesis starts with formation of 5-aminolevulinic acid (ALA) via the Shemin pathway, which involved condensation of glycine and succinyl-CoA (*15*). In mammalian cells, this step is catalysed by ALA synthase in the mitochondria. Next five steps in the cytosol and two final steps in the mitochondria take place, respectively. As shown in Supplementary Fig. S1, apicoplast, an additional compartment of *Plasmodium*, houses four haem synthesis enzymes (*9*). The last two enzymes, protoporphyrinogen IX oxidase and ferrochelatase (FC) are localized in the mitochondria.

In cancer cells, their uptake of a high concentration of ALA results in elevated levels of the metabolites particularly PPIX because of insufficient activity of FC (*16–19*). This accumulation of PPIX and other intermediates have led to the development of photodynamic diagnosis (PDD) and photodynamic therapy (PDT) of cancer. The principle behind the PDT rests on PPIX as a photosensitizer releasing singlet oxygen and other ROS leading to extensive cellular damages and cell death (*20*, *21*). Smith and Kain (2004) tried PDT to malaria parasites by ALA (*17*). Indeed, the growth of *P. falciparum* in blood culture was completely inhibited by 0.2 mM ALA followed by exposure to white light or by a higher concentration (2 mM) of ALA alone without light exposure. Unfortunately, direct adoption of ALA-PDT to malaria patient treatment is clinically unrealistic. However, in the present study, we found this pathway to be an attractive and promising target of malaria chemotherapy when ALA is supplemented with sodium ferrous citrate (SFC).

Plasmodium falciparum 3D7 strain was cultured and synchronous ring form was obtained as described previously (*22*). The haem intermediates were determined by HPLC according to the methods previously reported (*23*). Acyl carrier protein (ACP), the apicoplast marker, fused with GFP was used to locate the apicoplast (*24*, *25*). Details of the experimental procedures including organelle separation (*26*) are described in 'Supplementary Information'.

After extensive search of the previous reports on haem metabolism in *Plasmodium*, we studied effects of metal ions on the growth inhibition by ALA using human malaria parasite, *P. falciparum* 3D7. In fact, there was a report on protection from malaria by elevated zinc protoporphyrin, which binds to haem crystals to inhibit further crystallization to form haemozoin (*27*). In the first screening, iron was not examined because malaria infection impacts iron metabolism of the host in many diverse ways and debate on the effect of iron supplementation is still not clear (*14*). As shown in Fig. 1A, 10 μM $CoCl_2$ and $CuCl_2$ inhibited *P. falciparum* growth, while $MgCl_2$, $NiCl_2$, $ZnCl_2$ and $Pb(NO_3)_2$ did not show growth inhibition. However, in the presence of 200 μM of ALA, no significant difference from the experiments without ALA was observed, indicating that $CoCl_2$ and $CuCl_2$ do not synergistically enhance anti-malarial activity of ALA. Since none of those metal ions tested enhanced the growth inhibition of ALA, the effect of iron was examined next. Interestingly, the growth inhibition was increased to more than 50% when infected cells were treated with 10 μM SFC and 200 μM ALA, although SFC alone did not show any effect (Fig. 1A). The growth inhibition of the parasite by either ALA or SFC was dose-dependent (Supplementary Fig. S2). Similar effect was observed with $FeCl_2$ and $FeSO_4$ (data not shown). In contrast, oxidized iron such as ferric ammonium citrate, $FeCl_3$ and iron pyrophosphate did not inhibit the growth even in the presence of ALA, suggesting that only ferrous compounds have ability for synergy on ALA.

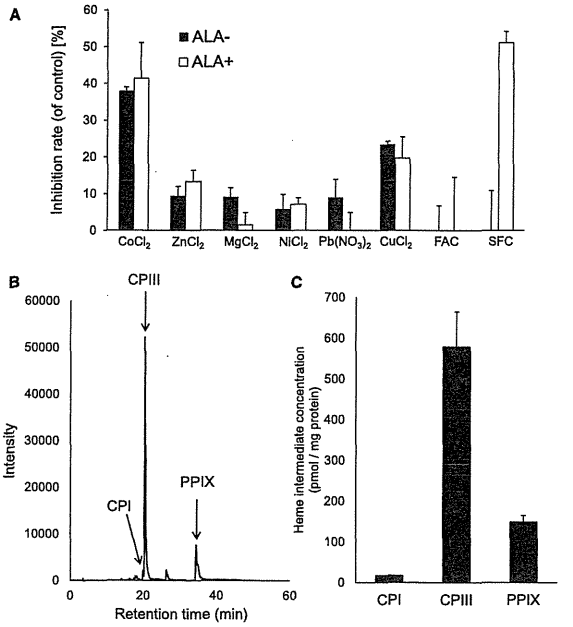

Fig. 1 Growth inhibition of *P. falciparum* by ALA and identification of haem intermediates. Parasite cultures treated with 5% (*w*/*v*) sorbitol were incubated for 72 h with different concentrations of ALA (0 and 200 μM) coupled with metal ions. (**A**) Parasite cultures added $CoCl_2$, $NiCl_2$, $MgCl_2$, $ZnCl_2$, $Pb(NO_3)_2$, FAC and SFC (10 μM) without (closed) or with (open) ALA. ($P < 0.01$) (**B**) The chromatograph obtained from HPLC analysis. Schizonts were collected after 24 h treatment of synchronized ring form with 200 μM ALA and 0.1 μM SFC. HPLC analysis is described in 'Materials and Methods' section in Supplementary Information. (**C**) Content of three intermediates. Concentrations of haem intermediates (per mg of protein) were calculated by fluorescence intensity of chromatograph.

To determine haem intermediates, the cell extract of the parasites obtained from culture was analysed by HPLC. As shown in Fig. 1B, the extract contained three major intermediates coproporphyrin I (CPI), coproporphyrin III (CPIII) and protoporphyrin IX (PPIX). CPIII was the most accumulated intermediate in *P. falciparum* (Fig. 1C). Accumulation of the haem intermediates was independent of SFC concentration after 24 h of ALA/SFC treatment (Supplementary Fig. S3) indicating that the combination of porphyrin accumulation and Fe^{2+} is required for the growth inhibition.

As the haem intermediates, including uroporphyrin III, CPIII, PPIX, are detectable by red fluorescence light, localization of the intermediates in the parasite treated with ALA and SFC was examined (Fig. 2A). In ring stage, the haem intermediates co-localized with GFP fused with ACP, which is an apicoplast marker (upper panel). In contrast, the haem intermediates co-localized with haemozoin in trophozoite and schizont stages (middle and lower panels), suggesting that the haem intermediates were localized to food vacuole at these stages.

To further confirm the localization of the intermediates in the organelles, fractions obtained by Percoll density gradient centrifugation after disruption of the cells by N_2-cavitation (*26*) were analysed (Fig. 2B).

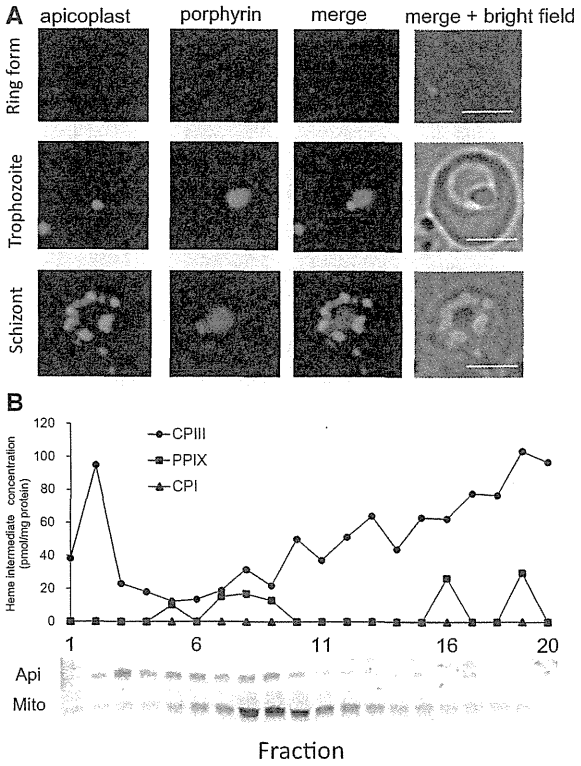

Fig. 2 Localization of haem intermediates. Parasites cultures were incubated for 24 h with 200 μM ALA and 0.1 μM SFC. (**A**) Analysis by fluorescence microscope. Haem intermediates were observed by blue (405–415 nm) excitation light. Apicoplast marker is GFP-fused ACP. Green: Apicoplast, Red: Haem intermediates and Scale bar is 5 μm. (**B**) Distribution of haem intermediates in the separated organelles. *Plasmodium falciparum* 3D7 organelles were separated by N_2-cavitation method (*22*) and percoll density centrifugation. Haem intermediates were determined by HPLC. Organelle in each fraction was detected by PCR. Api and Mito indicate the large subunit of rRNA gene encoded on apicoplast genome and subunit I of complex IV encoded on mitochondrion genome, respectively. CPI (triangle), CPIII (circle) and PPIX (square).

CPIII was predominantly accumulated in apicoplasts separated in the top fractions (2 and 3). PPIX was found in mitochondria (7–9). CPI, CPIII and PPIX were accumulated in the food vacuole, which contains haemozoin (21–23 in Supplementary Fig. S4A). CPIII and PPIX were accumulated in the RBC cytosol and medium, whereas only CPIII was accumulated in the parasite cytosol (Supplementary Fig. S4B). These results are consistent with the fluorescence microscopy observation except mitochondrial PPIX that was not detected by fluorescence microscopy due to relatively small amounts compared with CPIII.

The results presented here clearly show the growth inhibition of the malaria parasite by ALA/Fe^{2+} without light irradiation. However, mechanism of the growth inhibition is still unclear. One interesting result obtained is the suppression of ALA/Fe^{2+} growth inhibition of *P. falciparum* by ascorbate, a well-known anti-oxidant agent (Supplementary Fig. S5). Anti-oxidant effect of ascorbate suppressed growth inhibition of *P. falciparum* by ROS has been reported although *N*-acetyl-L-cysteine is weaker than ascorbate (*28*). Moreover, significant ROS production was observed by using 3-*p*-aminophenyl fluorescein (APF) in the parasites treated with ALA/Fe^{2+} (Supplementary Fig. S6). Since both low pH (lower than pH 3.0) and enough oxygen are essential for the Fenton reaction of iron with ascorbate (*29*, *30*), it is unlikely to occur with ascorbate in the parasite at neutral pH in the cytoplasm and low oxygen tension (5%) in the culture. In this regard, the synergy with ferrous but not ferric ion is quite interesting because iron has been discussed as a double-edged sword in the treatment of malaria patients (*14*). Exacerbation of malaria by iron supplement has been reported while an iron chelator, desferrioxamine, reduces the anti-malarial action of artemisinin. Similar to artemisinin, which is activated by Fenton reaction and produces ROS (*31*), the haem intermediates may interact with Fe^{2+} transported into the organelles by specific transporters (*32*) and release ROS, which damages DNA and membranes of organelles in the parasite. Different from the cancer cells, the main intermediate accumulated in *Plasmodium* was CPIII. This is due to the complex haem synthesis pathway in *Plasmodium* as shown in Supplementary Fig. S1. PPIX found in the mitochondria may also contribute to the growth inhibition with either Fe^{2+} or light irradiation.

We have already observed that ALA plus SFC rescued mice infected with *Plasmodium yoelii* (unpublished result). Furthermore, all of the preclinical data were evaluated by European Medicines Agency, and Phase I clinical study has been completed in 2013. Thus, the clinical study of commercially available ALA plus SFC on malaria is highly feasible.

Supplementary Data

Supplementary Data are available at *JB* Online.

Acknowledgements

This article is dedicated to Professor Kazuyuki Tanabe who has passed away on August 12, 2013. He has been leading scientist in the field of malaria research and always encouraging us.

Funding

This work was supported partly by a grant from the Program for Promotion of Basic and Applied Researches for Innovations in Bio-oriented Industry (BRAIN), Strategic Japanese-French Cooperative Program by JST, SATREPS (10000284), the Ministry of Health and Welfare for the Control of Emerging and Reemerging Diseases in Japan, and the UK Medical Research Council (MRC) (File: U117532067).

Conflict of interest

Tohru Tanaka is Chief Technology Officer and Motowo Nakajima is Chief Scientific Officer at SBI Pharmaceuticals Co., Ltd.

References

1. Snow, R.W., Guerra, C.A., Noor, A.M., Myint, H.Y., and Hay, S.I. (2005) The global distribution of clinical episodes of *Plasmodium falciparum* malaria. *Nature* **434**, 214–217

2. Cowman, A.F. and Crabb, B.S. (2006) Invasion of red blood cells by malaria parasites. *Cell* **124**, 755–766
3. Dondorp, A.M., Nosten, F., Yi, P., Das, D., Phyo, A.P., Tarning, J., Lwin, K.M., Ariey, F., Hanpithakpong, W., Lee, S.J., Ringwald, P., Silamut, K., Imwong, M., Chotivanich, K., Lim, P., Herdman, T., An, S.S., Yeung, S., Singhasivanon, P., Day, N.P., Lindegardh, N., Socheat, D., and White, N.J. (2009) Artemisinin resistance in *Plasmodium falciparum* malaria. *N. Engl. J. Med.* **361**, 455–467
4. Surolia, N. and Padmanaban, G. (1992) de novo biosynthesis of heme offers a new chemotherapeutic target in the human malarial parasite. *Biochem. Biophys. Res. Commun.* **187**, 744–750
5. Sigala, P.A., Crowley, J.R., Hsieh, S., Henderson, J.P., and Goldberg, D.E. (2012) Direct tests of enzymatic heme degradation by the malaria parasite *Plasmodium falciparum*. *J. Biol. Chem.* **287**, 37793–37807
6. Chugh, M., Sundararaman, V., Kumar, S., Reddy, V.S., Siddiqui, W.A., Stuart, K.D., and Malhotra, P. (2013) Protein complex directs hemoglobin-to-hemozoin formation in *Plasmodium falciparum*. *Proc. Natl Acad. Sci. USA* **110**, 5392–5397
7. Nagaraj, V.A., Sundaram, B., Varadarajan, N.M., Subramani, P.A., Kalappa, D.M., Ghosh, S.K., and Padmanaban, G. (2013) Malaria parasite-synthesized heme is essential in the mosquito and liver stages and complements host heme in the blood stages of infection. *PLoS Pathog.* **9**, e1003522
8. Kořený, L., Oborník, M., and Lukeš, J. (2013) Make it, take it, or leave it: heme metabolism of parasites. *PLoS Pathog.* **9**, e1003088
9. Sheiner, L., Vaidya, A.B., and McFadden, G.I. (2013) The metabolic roles of the endosymbiotic organelles of *Toxoplasma* and *Plasmodium spp. Curr. Opin. Microbiol.* **16**, 452–458
10. Heinemann, I.U., Jahn, M., and Jahn, D. (2008) The biochemistry of heme biosynthesis. *Arch. Biochem. Biophys.* **474**, 238–251
11. van Dooren, G.G., Kennedy, A.T., and McFadden, G.I. (2012) The use and abuse of heme in apicomplexan parasites. *Antioxid. Redox. Signal.* **17**, 634–656
12. Harada, S., Inaoka, D.K., Ohmori, J., and Kita, K. (2013) Diversity of parasite complex II. *Biochim. Biophys. Acta* **1827**, 658–667
13. Barton, V., Fisher, N., Biagini, G.A., Ward, S.A., and O'Neill, P.M. (2010) Inhibiting *Plasmodium* cytochrome *bc*1: a complex issue. *Curr. Opin. Chem. Biol.* **14**, 440–446
14. Scholl, P.F., Tripathi, A.K., and Sullivan, D.J. (2005) Bioavailable iron and heme metabolism in *Plasmodium falciparum*. *Curr. Top. Microbiol. Immunol.* **295**, 293–324
15. Shemin, D., Russell, C.S., and Abramsky, T. (1955) The succinate-glycine cycle. I. The mechanism of pyrrole synthesis. *J. Biol. Chem.* **215**, 613–626
16. Ohgari, Y., Miyata, Y., Miyagi, T., Gotoh, S., Ohta, T., Kataoka, T., Furuyama, K., and Taketani, S. (2011) Roles of porphyrin and iron metabolisms in the δ-aminolevulinic acid (ALA)-induced accumulation of protoporphyrin and photodamage of tumor cells. *Photochem. Photobiol.* **87**, 1138–1145
17. Smith, T.G. and Kain, K.C. (2004) Inactivation of *Plasmodium falciparum* by photodynamic excitation of heme-cycle intermediates derived from delta-aminolevulinic acid. *J. Infect. Dis.* **190**, 184–191
18. Amo, T., Kawanishi, N., Uchida, M., Fujita, H., Oyanagi, E., Utsumi, T., Ogino, T., Inoue, K., Shuin, T., Utsumi, K., and Sasaki, J. (2009) Mechanism of cell death by 5-aminolevulinic acid-based photodynamic action and its enhancement by ferrochelatase inhibitors in human histiocytic lymphoma cell line U937. *Cell. Biochem. Funct.* **27**, 503–515
19. Ohgari, Y., Nakayasu, Y., Kitajima, S., Sawamoto, M., Mori, H., Shimokawa, O., Matsui, H., and Taketani, S. (2005) Mechanisms involved in delta-aminolevulinic acid (ALA)-induced photosensitivity of tumor cells: relation of ferrochelatase and uptake of ALA to the accumulation of protoporphyrin. *Biochem. Pharmacol.* **71**, 42–49
20. Dougherty, T.J., Gomer, C.J., Henderson, B.W., Jori, G., Kessel, D., Korbelik, M., Moan, J., and Peng, Q. (1998) Photodynamic therapy. *J. Natl. Cancer. Inst.* **90**, 889–905
21. Kimura, M., Itoh, Y., Tokuoka, Y., and Kawashima, N. (2004) Delta-aminolevulinic acid-based photodynamic therapy for acne on the body. *J. Dermatol.* **31**, 956–960
22. Trager, W. and Jensen, J.B. (1976) Human malaria parasites in continuous culture. *Science* **193**, 673–675
23. Hagiya, Y., Adachi, T., Ogura, S., An, R., Tamura, A., Nakagawa, H., Okura, I., Mochizuki, T., and Ishikawa, T. (2008) Nrf2-dependent induction of human ABC transporter ABCG2 and heme oxygenase-1 in HepG2 cells by photoactivation of porphyrins: biochemical implications for cancer cell response to photodynamic therapy. *J. Exp. Ther. Oncol.* **7**, 153–167
24. Sato, S. and Wilson, R.J. (2004) The use of DsRED in single- and dual-color fluorescence labeling of mitochondrial and plastid organelles in *Plasmodium falciparum*. *Mol. Biochem. Parasitol.* **134**, 175–179
25. Sato, S., Rangachari, K., and Wilson, R.J. (2003) Targeting GFP to the malarial mitochondrion. *Mol Biochem Parasitol* **130**, 155–158
26. Kobayashi, T., Sato, S., Takamiya, S., Komaki-Yasuda, K., Yano, K., Hirata, A., Onitsuka, I., Hata, M., Miichi, F., Tanaka, T., Hase, T., Miyajima, A., Kawazu, S., Watanabe, Y., and Kita, K. (2007) Mitochondria and apicoplast of *Plasmodium falciparum*: behaviour on subcellular fractionation and the implication. *Mitochondrion* **7**, 125–132
27. Iyer, J.K., Shi, L., Shankar, A.H., and Sullivan, D.J. (2003) Zinc protoporphyrin IX binds heme crystals to inhibit the process of crystallization in *Plasmodium falciparum*. *Mol. Med.* **9**, 175–182
28. Njomnang Soh, P., Witkowski, B., Gales, A., Huyghe, E., Berry, A., Pipy, B., and Benoit-Vical, F. (2012) Implication of glutathione in the *in vitro* antiplasmodial mechanism of action of ellagic acid. *PLoS One* **7**, e45906
29. Samuni, A., Aronovitch, J., Godinger, D., Chevion, M., and Czapski, G. (1983) On the cytotoxicity of vitamin C and metal ions. A site-specific Fenton mechanism. *Eur. J. Biochem.* **137**, 119–124
30. Winter, R.W., Ignatushchenko, M., Ogundahunsi, O.A., Cornell, K.A., Oduola, A.M., Hinrichs, D.J., and Riscoe, M.K. (1997) Potentiation of an antimalarial oxidant drug. *Antimicrob. Agents. Chemother.* **41**, 1449–1454
31. Araújo, J.Q., Carneiro, J.W., de Araujo, M.T., Leite, F.H., and Taranto, A.G. (2008) Interaction between artemisinin and heme. A Density Functional Theory study of structures and interaction energies. *Bioorg. Med. Chem.* **16**, 5021–5029
32. Seeber, F. and Soldati-Favre, D. (2010) Metabolic pathways in the apicoplast of apicomplexa. *Int. Rev. Cell. Mol. Biol.* **281**, 161–228

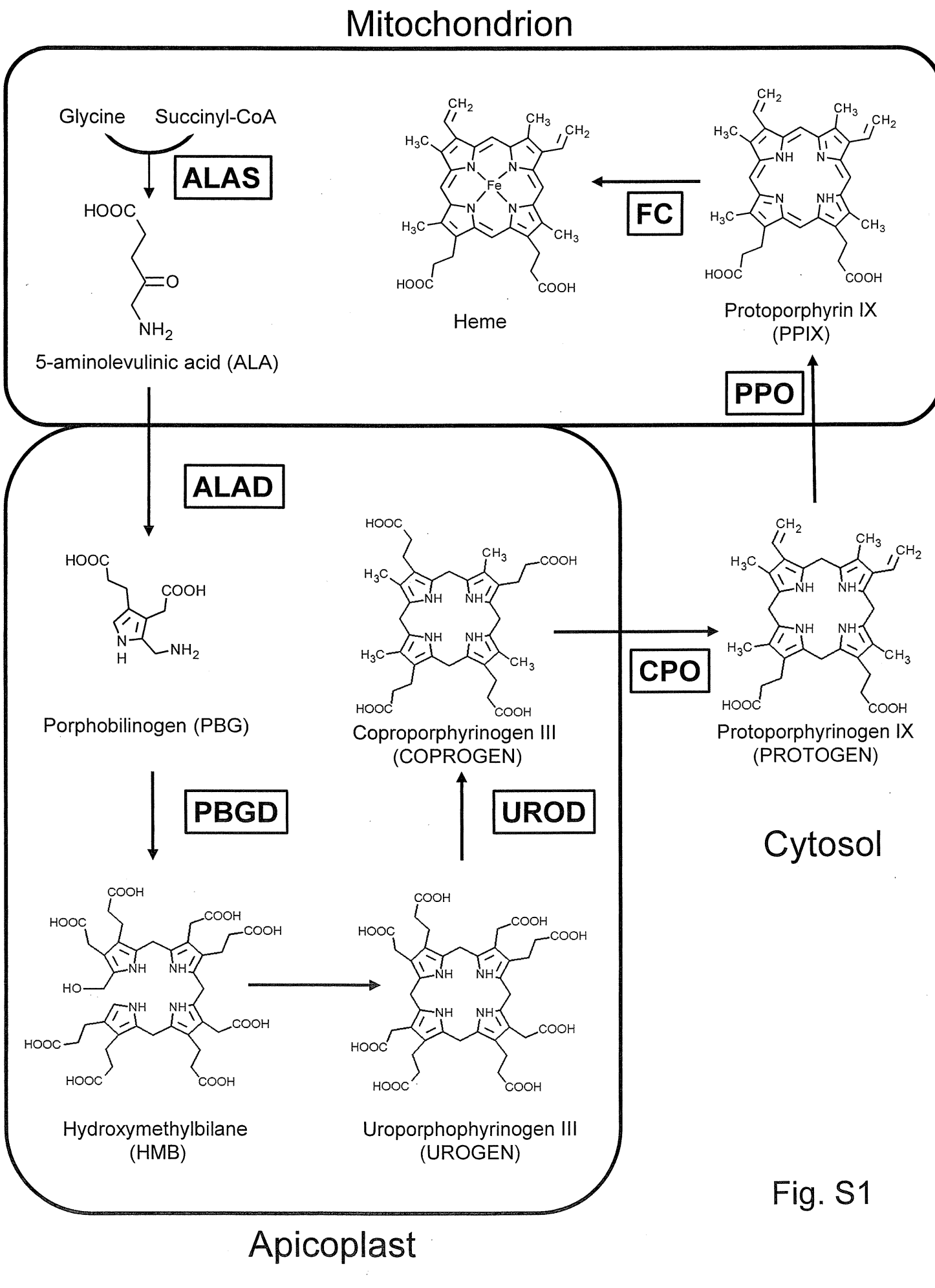
Mitochondrion
Glycine
Succinyl-CoA
ALAS
5-aminolevulinic acid (ALA)
Heme
FC
Protoporphyrin IX
(PPIX)
PPO
ALAD
Porphobilinogen (PBG)
Coproporphyrinogen III
(COPROGEN)
CPO
Protoporphyrinogen IX
(PROTOGEN)
Cytosol
PBGD
UROD
Hydroxymethylbilane
(HMB)
Uroporphophyrinogen III
(UROGEN)
Apicoplast

Fig. S1

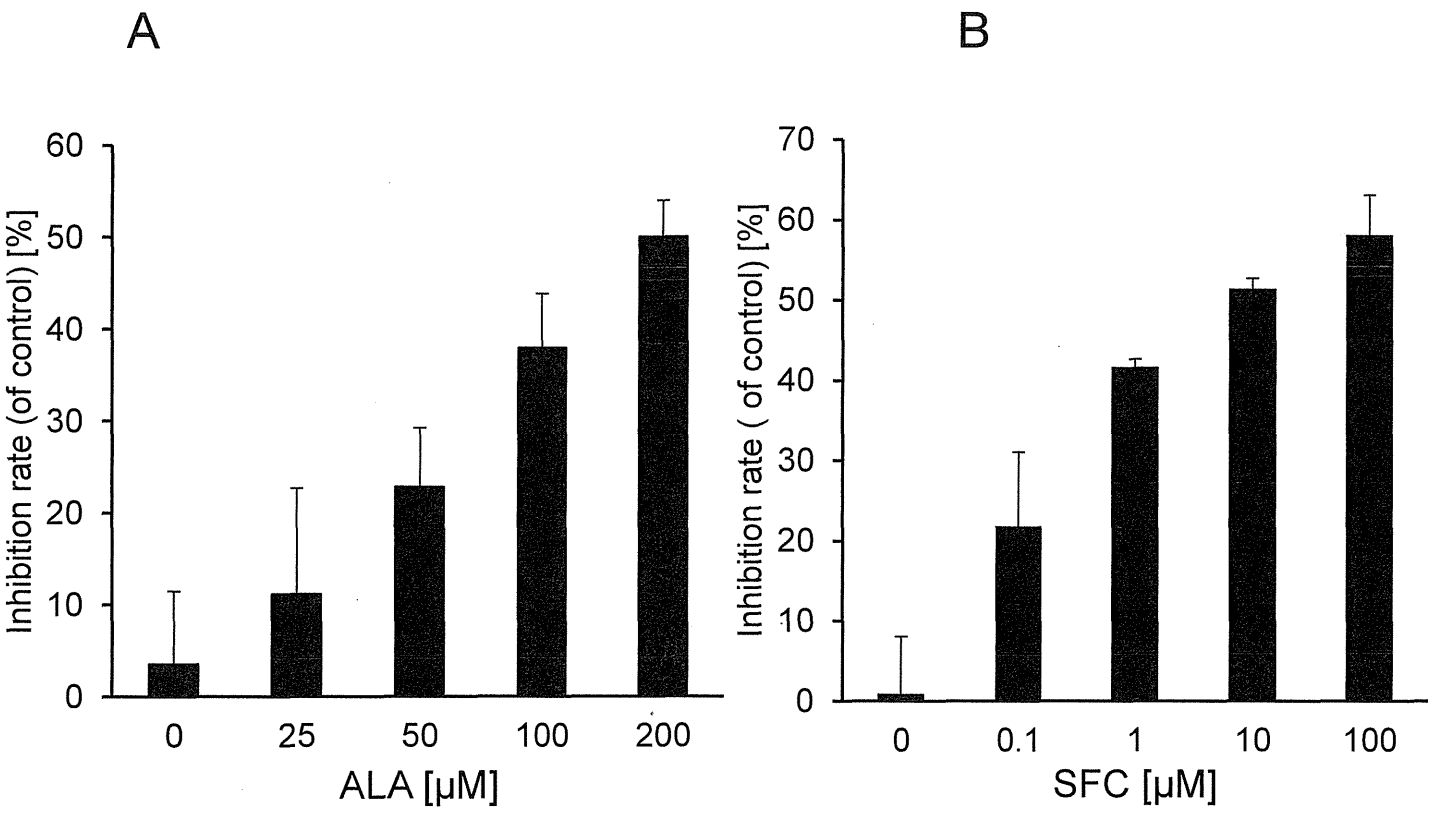
A
B
Inhibition rate (of control) [%]
60
50
40
30
20
10
0
0
25
50
100
200
ALA [μM]
Inhibition rate (of control) [%]
70
60
50
40
30
20
10
0
0
0.1
1
10
100
SFC [μM]

Fig. S2

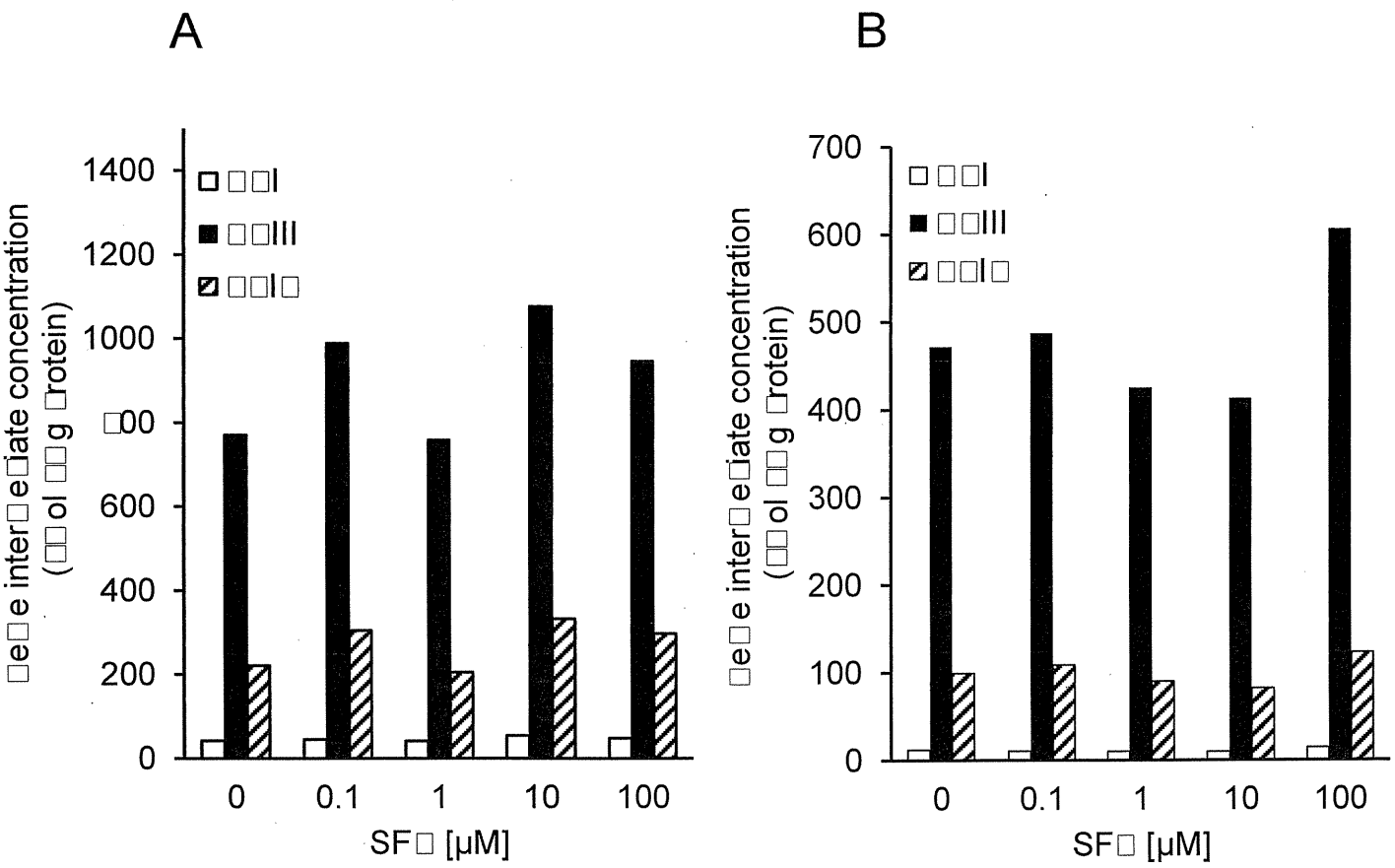
A
B
1400
1200
1000
600
400
200
0
700
600
500
400
300
200
100
0
0
0.1
1
10
100
SF [μM]

Fig. S3

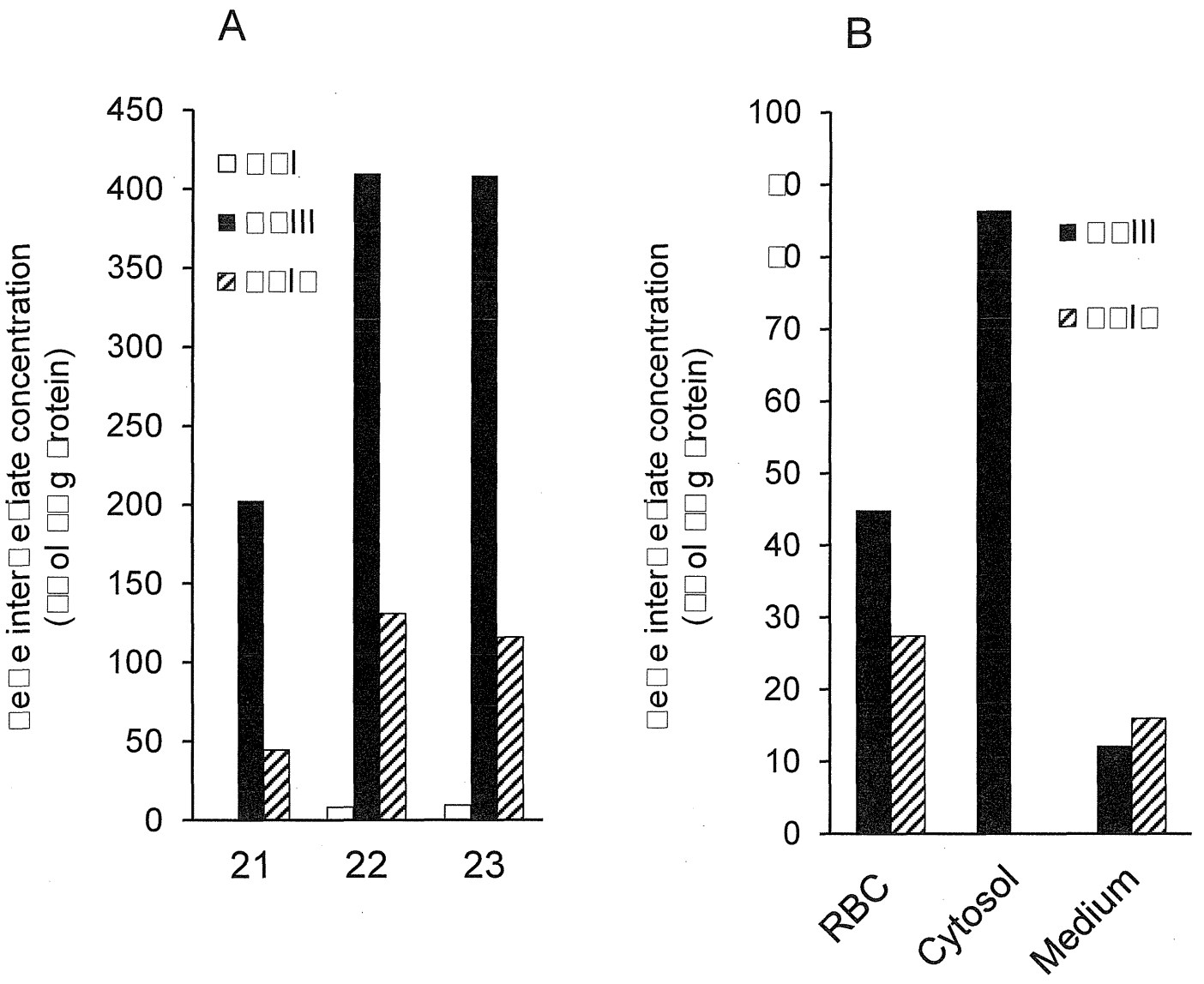
A
450
400
350
300
250
200
150
100
50
0
21
22
23
B
100
70
60
50
40
30
20
10
0
RBC
Cytosol
Medium

Fig. S4

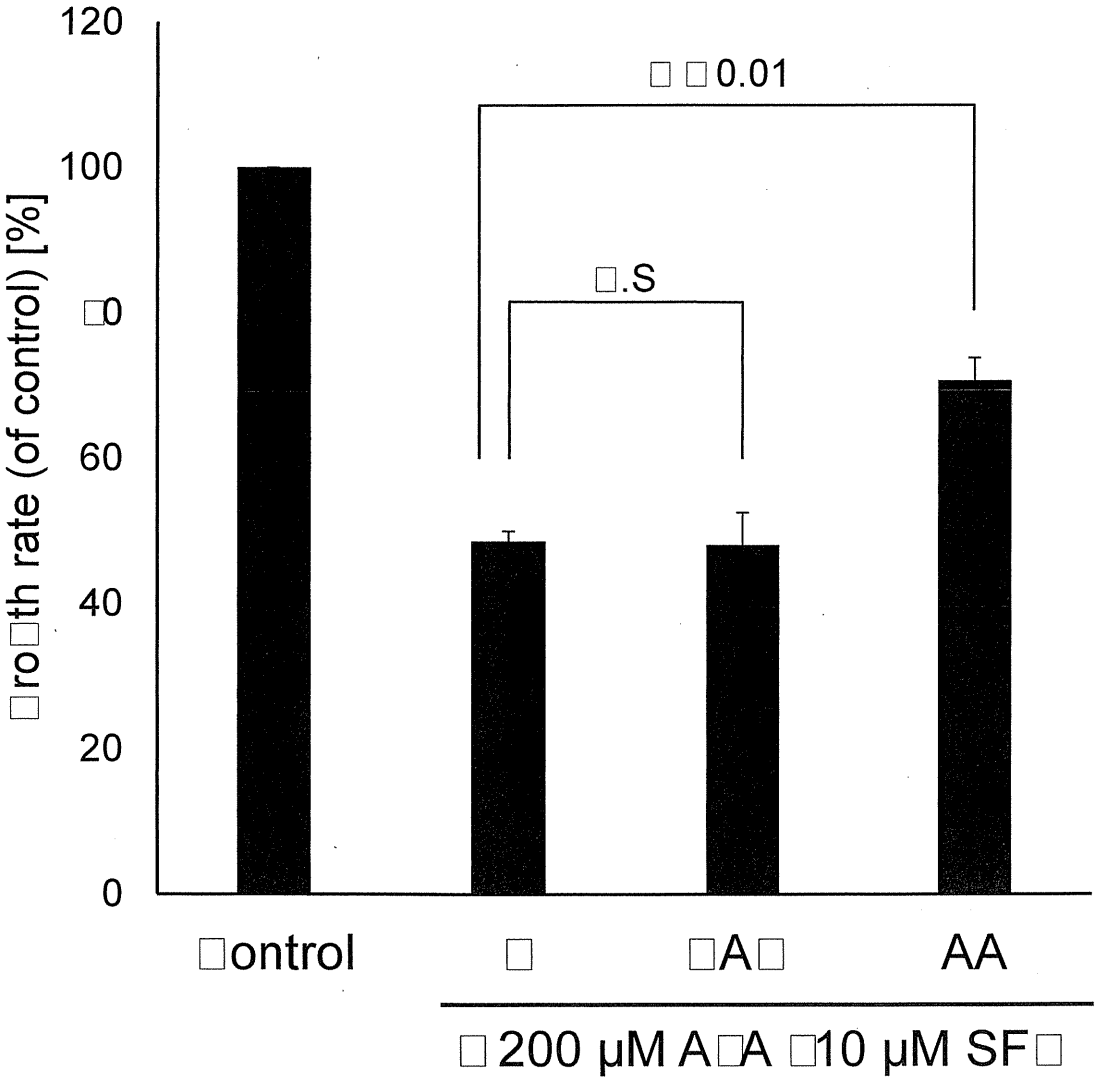
120
100
□0
60
40
20
0
□ro□th rate (of control) [%]
□ □0.01
□.S
□ontrol
□
□A□
AA
□ 200 μM A□A □10 μM SF□

Fig. S5

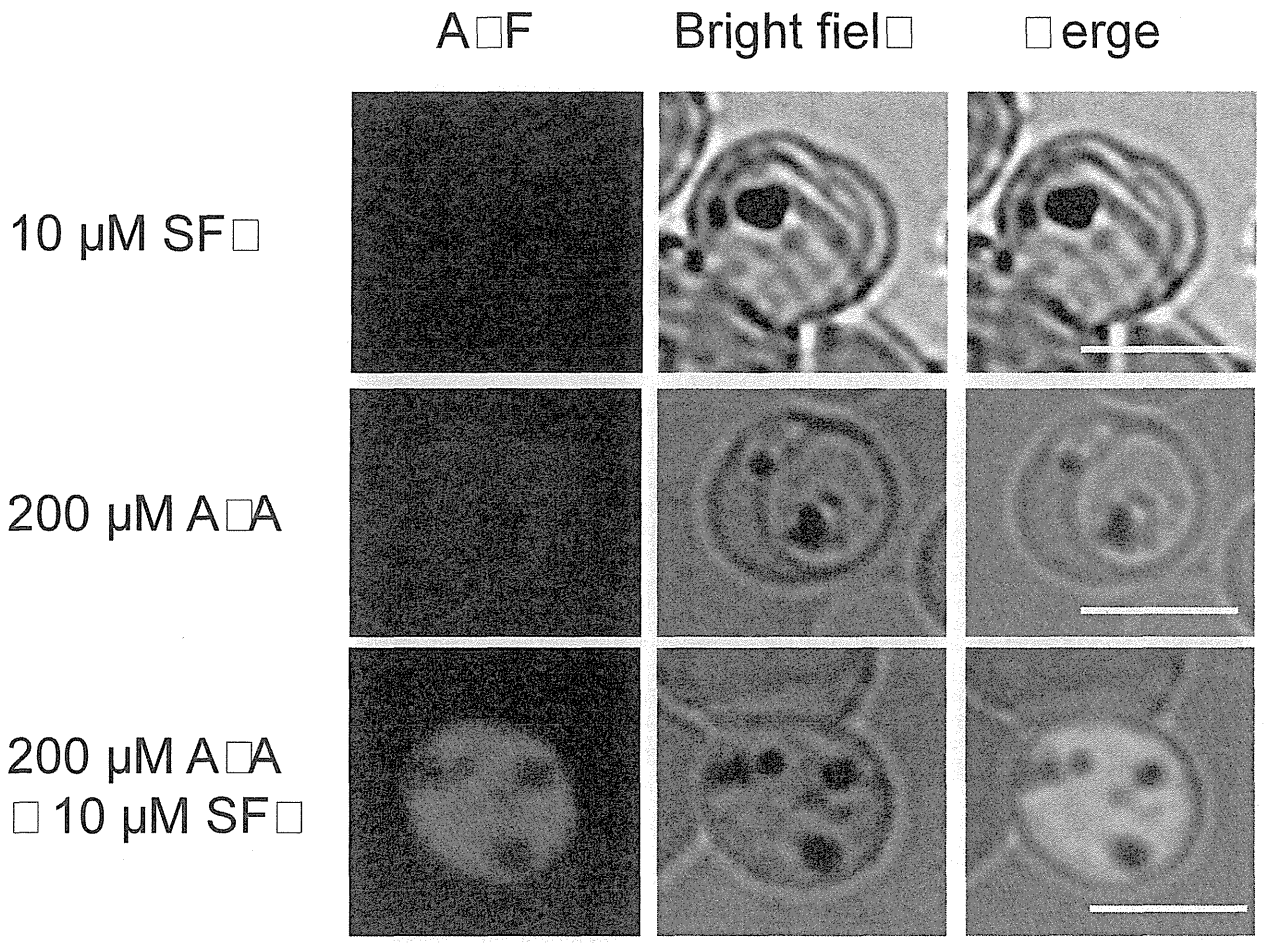

Fig. S6

Biochimica et Biophysica Acta 1827 (2013) 658–667

Contents lists available at SciVerse ScienceDirect

Biochimica et Biophysica Acta

journal homepage: www.elsevier.com/locate/bbabio

Review

Diversity of parasite complex II☆

Shigeharu Harada [a,*], Daniel Ken Inaoka [b], Junko Ohmori [b], Kiyoshi Kita [b,**]

[a] Department of Applied Biology, Graduate School of Science and Technology, Kyoto Institute of Technology, Kyoto 606-8585, Japan
[b] Department of Biomedical Chemistry, Graduate School of Medicine, The University of Tokyo, Tokyo 113-0033, Japan

ARTICLE INFO

Article history:
Received 16 October 2012
Received in revised form 7 January 2013
Accepted 9 January 2013
Available online 16 January 2013

Keywords:
Complex II
Fumarate respiration
Ascaris suum
Trypanosoma cruzi
Chemotherapy
Drug design

ABSTRACT

Parasites have developed a variety of physiological functions necessary for completing at least part of their life cycles in the specialized environments of surrounding the parasites in the host. Regarding energy metabolism, which is essential for survival, parasites adapt to the low oxygen environment in mammalian hosts by using metabolic systems that are very different from those of the hosts. In many cases, the parasite employs aerobic metabolism during the free-living stage outside the host but undergoes major changes in developmental control and environmental adaptation to switch to anaerobic energy metabolism. Parasite mitochondria play diverse roles in their energy metabolism, and in recent studies of the parasitic nematode, *Ascaris suum*, the mitochondrial complex II plays an important role in anaerobic energy metabolism of parasites inhabiting hosts by acting as a quinol-fumarate reductase. In Trypanosomes, parasite complex II has been found to have a novel function and structure. Complex II of *Trypanosoma cruzi* is an unusual supramolecular complex with a heterodimeric iron–sulfur subunit and seven additional non-catalytic subunits. The enzyme shows reduced binding affinities for both substrates and inhibitors. Interestingly, this structural organization is conserved in all trypanosomatids. Since the properties of complex II differ across a wide range of parasites, this complex is a potential target for the development of new chemotherapeutic agents. In this regard, structural information on the target enzyme is essential for the molecular design of drugs. This article is part of a Special Issue entitled: Respiratory complex II: Role in cellular physiology and disease.

1. Introduction

1.1. Molecular parasitology

Parasites are classified generally as either helminths or protozoans. Helminths are multi-cellular parasites and are divided into three types: nematodes (e.g., *Ascaris suum*), trematodes (e.g., *Schistosoma japonica*), and cestodes (e.g., *Diphyllobothrium latum*). Protozoans include unicellular parasites (e.g., malaria parasites and *Entamoeba histolytica*), but they differ from bacteria in that they have a nucleus, mitochondria, vacuole, and other organelles (e.g., apicoplast, hydrogenosomes, and mitosomes). These parasites are capable of surviving and proliferating due to avoidance of host defense mechanisms and development of metabolic pathways adapted to the specialized environments of the host [see reviews 1–5].

Studies of parasitic adaptation have yielded extremely informative biological discoveries and data that are potentially useful for developing treatments of infectious diseases. Recent advances in biochemistry and molecular biology have provided new insights into basic parasite biology and have led to many revolutionary discoveries concerning biological evolution and diversity. Taken together, a new field called 'molecular parasitology' is being established to investigate parasitism at the molecular level. The unique features of parasite complex II have been revealed through data obtained through such a pioneering sciences [1,4,5].

1.2. Functional and subunit changes of complex II during the A. suum life cycle

The nematode *A. suum* has been studied extensively as a representative of human and livestock parasites [1]. During its life cycle, *A. suum* transitions from aerobic to anaerobic metabolism, reflecting the change in the environmental oxygen concentration (Fig. 1) [2–7]. During development from a fertilized egg to third stage larvae (L3) outside of the host, metabolism is aerobic as the tissues of mammalian host in that ATP is synthesized by aerobic oxidative phosphorylation [8]. In contrast,

Abbreviations: PEPCK, phosphoenolpyruvate carboxykinase; RQ, rhodoquinone; QFR, quinol-fumarate reductase; Fp, flavoprotein; FAD, flavin adenine dinucleotide; Ip, iron–sulfur protein; CybL, large subunit ofcytochrome *b*; CybS, small subunit of cytochrome *b*; SDH, succinate dehydrogenase; UQ, ubiquinone; SQR, succinate-ubiquinone reductase; MK, menaquinone; RQH_2, rhodoquinol; FRD, fumarate reductase; OAA, oxaloacetate

☆ This article is part of a Special Issue entitled: Respiratory complex II: Role in cellular physiology and disease.

* Correspondence to: S. Harada, Department of Applied Biology, Graduate School of Science and Technology, Kyoto Institute of Technology, Sakyo-ku, Kyoto 606-8585, Japan. Tel.: +81 75 724 7541; fax: +81 75 724 7541.
** Correspondence to: K. Kita, Department of Biomedical Chemistry, Graduate School of Medicine, The University of Tokyo, Hongo, Bunkyo-ku, Tokyo 113-0033, Japan. Tel.: +81 3 5841 3526; fax: +81 3 5841 3444.
E-mail addresses: harada@kit.ac.jp (S. Harada), kitak@m.u-tokyo.ac.jp (K. Kita).

0005-2728/$ – see front matter © 2013 Published by Elsevier B.V.
http://dx.doi.org/10.1016/j.bbabio.2013.01.005

adult worms, which live in a low-oxygen environment, use the anaerobic phosphoenolpyruvate carboxykinase (PEPCK)-succinate pathway. The last step of the PEPCK-succinate pathway involves the NADH-fumarate reductase system, which is composed of complex I (NADH-quinone reductase), low-potential rhodoquinone (RQ), and complex II (quinol-fumarate reductase, QFR) [4,9]. Electron transfer from NADH to fumarate is coupled to ATP synthesis by site I phosphorylation in complex I. The difference in redox potential between NAD^+/NADH ($Em' = -320$ mV) and fumarate/succinate ($Em' = +30$ mV) is sufficient to drive ATP synthesis [4].

In eukaryotes, complex II is localized in the inner mitochondrial membrane and is generally composed of four peptides [4]. The largest flavoprotein (Fp, SDHA) subunit has a molecular mass of about 70 kDa and contains flavin adenine dinucleotide (FAD) as a prosthetic group. The relatively hydrophilic catalytic region of complex II is formed by the Fp subunit and the iron–sulfur cluster (Ip, SDHB) subunit, which has a molecular weight of about 30 kDa. The remaining subunits comprise cytochrome *b*, which contains heme *b*. Cytochrome *b* is composed of 2 hydrophobic membrane-anchoring polypeptide subunits: the 15 kDa large subunit (CybL, SDHC) and the 13 kDa small subunit (CybS, SDHD). These cytochrome *b* subunits are necessary for the interaction between complex II and hydrophobic membrane-associated quinones, such as ubiquinone (UQ) and RQ [6].

In a previous study, we showed that *A. suum* mitochondria express stage-specific isoforms of complex II [6,7,10]. While there are no differences in the isoforms of the Ip and CybL subunits of complex II between L3 larvae and adult *A. suum*, there are different isoforms of the complex II subunits Fp (larval, Fp^L; adult, Fp^A) and CybS (larval, $CybS^L$; adult, $CybS^A$) [7]. Quinone species in the mitochondria also differ during the life cycle of *A. suum*. In the adult mitochondria, the predominant quinone is the low-potential RQ ($Em' = -63$ mV); in larvae, the predominant quinone is UQ ($Em' = +110$ mV) [11]. Similarly, *Escherichia coli* and other bacteria show shifts in the combination of succinate-ubiquinone reductase (SQR) and UQ, and that of QFR and a low-potential quinone, such as menaquinone (MK) or RQ, during metabolic adaptation to changes in oxygen supply [12,13]. UQ has a higher redox potential than RQ; therefore, RQ is better suited to transferring electrons to fumarate than is UQ. In L2 and L3 *A. suum* larvae, UQ preferentially donates electrons to the cytochrome chain in the mitochondria. Thus, UQ participates in aerobic metabolism in *A. suum* larvae, whereas RQ participates in anaerobic metabolism in adult *A. suum* [11].

After being ingested by the definitive host, the L3 larvae penetrate the intestinal wall and reach the lung by migrating through other tissues, such as liver and heart. The L3 larvae pass from the lung via the trachea to the small intestine where they molt to L4 and develop into sexually maturate adult worms in the small intestine [14]. Protein chemical analysis reveals that the change in complex II begins with the anchor CybS subunit and then the Fp subunit [15].

1.3. Parasite complex II

Complex II molecules are classified into four types (Type A–D) and three classes (Class 1–3) according to the architecture of membrane anchors and functions *in vivo*, respectively [16]. The membrane anchor of Type A complex II consists of two polypeptide chains each having three transmembrane helices and two protoheme IX (heme *b*) molecules. Type B has one polypeptide chain with five transmembrane helices and two heme *b* molecules. On the other hand, Type C and D, like Type A, consist of two polypeptide chains with one and no heme *b* molecules in their anchors, respectively. In addition, more recent physiological analysis indicates novel Type E complex II [17], which is different from Type A–D in membrane-anchoring subunits and the composition of iron–sulfur centers. Class 1 complex II functions as SQR *in vivo* and catalyzes the oxidation of succinate and the reduction of high potential quinone, typically ubiquinone, whereas Class 2 complex II (QFR) catalyzes the opposite reaction, the oxidation of low potential quinol such as menaquinol and rhodoquinol (RQH_2) and the reduction of fumarate. Complex II belonging to Class 3, like the Class 1 enzymes, exhibits SQR activity but reduces low potential quinone. Crystal structures of complex II have been determined for three QFRs from *E. coli* (pdb code, 1L0V; [18]), *Wolinella succinogenes* (1QLB; [19]) and *A. suum* (3VR8; [20]), three SQRs from *E. coli* (1NEK; [21]), porcine (1ZOY; [22]) and chicken (1YQ3; [23]). QFRs from *E. coli*, *W. succinogenes*, and *A. suum* belong to Type D, Type B and Type C,

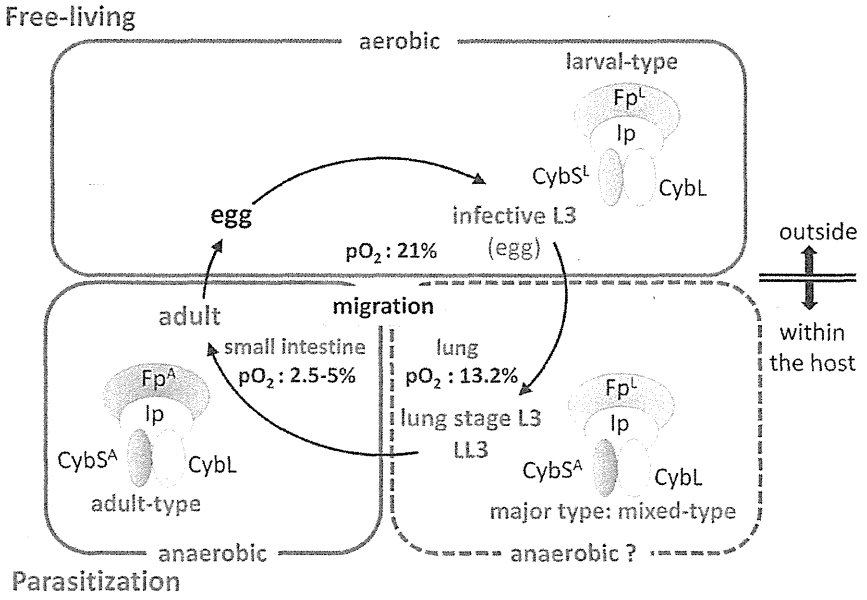

Fig. 1. Life cycle of *A. suum*. Fertilized eggs grow to infective L3 under an aerobic environment. Infective L3 larvae are ingested by the host, reach the small intestine and hatch there. Afterwards, larvae migrate into the host body (liver, heart, lung, and pharynx), and finally migrate back to the small intestine and develop into adults. In the host small intestine, the oxygen concentration is only 2.5% to 5% of that of the exogenous environment. During the life cycle, complex II molecules are expressed as stage-specific isoforms, larval-type, mixed-type and adult-type [15].

respectively, whereas SQRs from porcine, chicken and *E. coli* are the Type C enzymes.

In general, the complex II molecules of helminthes, which are multi-cellular parasites, are of Type C, although catalytic function changes during the life cycle as mentioned above. However, complex II purified from the parasitic protist, *Trypanosoma cruzi*, consists of six hydrophilic and six hydrophobic nuclear-encoded subunits [24]. Notably, the iron–sulfur subunit is heterodimeric; $SDH2_N$ and $SDH2_C$ contain plant-type ferredoxin domains in the *N*-terminal half and bacterial ferredoxin domains in the C-terminal half, respectively.

In the case of malaria parasites, such as *Plasmodium falciparum*, anchor subunits of complex II have not yet been identified, although the enzyme shows SQR activity [25]. These unusual features of parasite complex II molecules make them targets for new chemotherapeutic agents.

In this review, we mainly focus on recent advances in the study of *A. suum* complex II, which plays an important role in the anaerobic energy metabolism of parasites. In addition, the molecular architecture of 12 novel complex II subunits of *T. cruzi* will be discussed.

2. Structure of adult *A. suum* QFR

Anaerobic mitochondrial complex II from adult *A. suum* (*A. suum* QFR) belongs to Type C/Class 2 and couples the oxidation of RQH_2 to RQ to the reduction of fumarate to succinate, an opposite reaction catalyzed by SQR of the aerobic respiratory chain [7]. We crystallized *A. suum* QFR in the presence of malonate [26], a well-known competitive inhibitor against complex II in various organisms and determined the crystal structure at 2.8 Å resolution (3VR8; [20]) by molecular replacement using the structure of porcine SQR (1ZOY; [22]) as the search model. In addition, the structure of the ternary complex with fumarate and flutolanil was determined at 2.9 Å resolution (3VRB; [20]). Flutolanil is a widely used commercially available fungicide [27] that specifically inhibits *A. suum* QFR as shown by IC_{50} values for *A. suum* QFR of 58 nM and porcine SQR of 46 μM. Based on these structures, as well as the structure of porcine SQR in complex with flutolanil (3AE8), the enzymatic mechanism of *A. suum* QFR and the structural basis of the specificity of flutolanil against *A. suum* QFR will be discussed.

2.1. Overall structure

The structure of *A. suum* QFR, the first eukaryotic Type C/Class 2 complex II molecule to be characterized, is composed of four protein subunits (Fig. 2A): hydrophilic Fp (residues A33–A645) and Ip (B33–B281) subunits, and membrane-anchoring hydrophobic CybL (C34–C186) and CybS (D28–D156) subunits [20]. Several terminal residues of each mature polypeptide (Fp: A31–A645, Ip: B29–B282, CybL: C32–C188 and CybS: D26–D156) are missing in the current model because of faint electron density. The enzyme accommodates five prosthetic groups: a FAD molecule, three ion-sulfur centers ([2Fe–2S], [4Fe–4S], [3Fe–4S]), and one heme *b* molecule (Fig. 2B). Although there are two molecules in the asymmetric unit, *A. suum* QFR, like *E. coli* QFR [18], porcine SQR [22] and chicken SQR [23], exists as a monomer both in solution and crystal, which distinguishes the enzyme from the reported dimer structure of *W. succinogenes* QFR [19] and the trimer structure of *E. coli* SQR [21]. Further, the amino acid sequence of each subunit of *A. suum* QFR (Fig. 3) shows higher identity with porcine and chicken SQRs than with *E. coli* SQR and *E. coli* and *W. succinogenes* QFRs. Accordingly, *A. suum* QFR is more closely related to porcine and chicken SQRs rather to *E. coli* and *W. succinogenes* bacterial complex IIs. The arrangement of the bound prosthetic groups in the *A. suum* QFR structure [20] is similar to that of other complex IIs with known structures [18,19,21–23]. The chain of the FAD, [2Fe–2S], [4Fe–4S] and [3Fe–4S] prosthetic groups is disposed between dicarboxylate- and quinone-binding sites with the distances between neighboring centers less than 14 Å (Fig. 2B), suggesting that electron transfer from RQH_2 to FAD is carried out by quantum tunneling [28], as proposed for *E. coli* SQR [21].

2.2. Fp subunit

The largest Fp subunit of *A. suum* QFR [20] folds into four domains (Fig. 4A): a FAD-binding domain (residues A33–A280 and A380–A465), a capping domain (A281–A379), a helical domain (A466–A568), and a C-terminal domain (A569–A645). The FAD molecule forms a covalent bond with His A79 and hydrogen bonds primarily with main-chain N atoms of highly conserved residues of the FAD-binding domain (A49, A71, A72, A73, A78, A80, A84, A85, A86, A201, A255, A421, A432, A437 and A438). In addition, residues within 5 Å of the FAD group, especially those close to the FAD isoalloxazine ring, are highly conserved (Fig. 3A).

Examination of the refined structure shows significant electron density near the isoalloxazine ring that can be assigned as malonate, an additive for crystallization [20]. The location of this site is in agreement with the dicarboxylate-binding site assigned to other complex IIs with known structures [18,19,21–23] and is constructed by residues of the FAD-binding domain (A84, A85, A153, A276, A387, A432 and A435) and the capping domain (A286, A288, A289 and A320). Three basic residues, Arg A320, His A387 and Arg A432, interact with the C3 carboxylate group of the bound malonate, and Thr A288 and Arg A320 with the C1 carboxylate group (Fig. 4A). With the exception of A84, A153 and A435, these residues are conserved across complex II molecules with known structures (Fig. 3A).

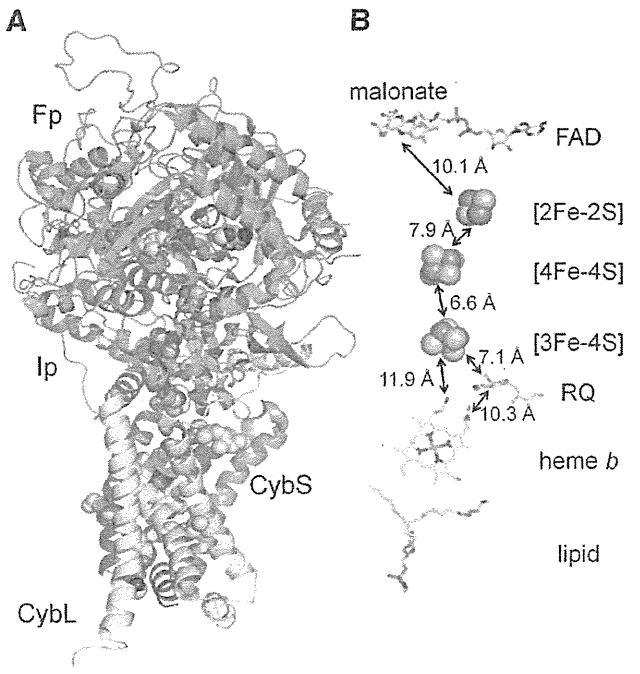

Fig. 2. Overall structure of *A. suum* QFR. (A) Cartoon representation of the overall structure of *A. suum* QFR. FAD-binding subunit (Fp) is shown in green; iron–sulfur subunit (Ip) is shown in cyan; and the transmembrane subunits CybL and CybS are shown in yellow and orange, respectively. The intrinsic redox centers (FAD, [2Fe–2S], [4Fe–4S], [3Fe–4S] and heme *b*) and bound small molecules (malonate, rhodoquinone, and lipid) are shown as spheres. (B) The arrangement of the redox centers together with malonate, rhodoquinone and lipid, and edge-to-edge distances between adjacent redox centers. For calculation of edge-to-edge distances, the dominant determinants of the electron tunneling rate, the sulfur atoms of the cysteine residues ligating to the iron–sulfur centers are included as part of the redox centers. The FAD edge is the isoalloxazine ring system and the heme edge is the conjugated macrocycle. Color-coding for each atom type is as follows: C, white; N, blue; O, red; S, dark yellow; and Fe, brown.

Fig. 3. Amino acid sequences of *A. suum* SQR. (A) Fp, (B) Ip, (C) CybL, and (D) CybS subunits. Residues conserved in the six complex II molecules with known structures (SQRs from porcine, chicken, and *E. coli* and QFRs from *E. coli*, *W. succinogenes*, and *A. suum*) are highlighted in red, residues conserved in SQRs from porcine, chicken, and *E. coli* and *A. suum* QFR are highlighted in green, residues conserved in porcine and chicken SQRs and *A. suum* QFR are highlighted in blue. Residues within 5 Å of FAD, [2Fe–2S], [4Fe–4S], [3Fe–4S], rhodoquinone and heme *b* redox centers are marked by *, 2, 4, 3, q, and h, respectively.

2.3. *Ip subunit*

The Ip subunit (Fig. 4B) is constructed by two domains, a plant ferredoxin-like N-terminal (B33–B130) and a bacterial ferredoxin-like C-terminal (B131–B281) domain [20]. The [2Fe–2S] center is bound to the N-terminal domain through coordination bonds with four cysteine residues (B89, B94, B97, and B109). The [4Fe–4S] and [3Fe–4S] centers are bound to the C-terminal domain and are coordinated by four (B182, B185, B188, and B249) and three (B192, B239, and B245) cysteine residues, respectively. Except for Cys B97, which is replaced by aspartate (Asp B63) in *E. coli* SQR [21], the cysteine residues are conserved (Fig. 3B). Out of 47 residues located within 5 Å of the iron–sulfur center of *A. suum* QFR [20], 44 residues are conserved in porcine and chicken SQRs, but that number decreases to 20 residues when compared across all complex II molecules with known structures [18,19,21–23]. The sulfur atoms of the cysteine ligands of [2Fe–2S] and [4Fe–4S] form –S:···H–N< interactions with main-chain amino groups of the N-terminal domain (B91, B92, B93, B96, and B108) and C-terminal domain (B184, B186, B187, B189, and B251), respectively. In addition, sulfur atoms of the iron–sulfur centers interact with the Ip subunit: the [2Fe–2S] center interacts with B90 N and B95 N, the [4Fe–4S] center with B183 N and B186 N, and the [3Fe–4S] center with B243 N. The –S:···H–N< interaction is also found in other complex II molecules [18, 19, 21–23, pdb code: 1L0V, 1QLB, 1NEK, 1ZOY and 1YQ3] and could affect the basicity of sulfur atoms of the cysteine ligands and the redox centers. It is worth noting that side chain atoms of Ser B96, Cys B187, and Tyr B202 interact with sulfur atoms of Cys B94, Cys B185, and [3Fe–4S], respectively (Fig. 4B). Although these residues are conserved in porcine and chicken complex II molecules (Fig. 3), Cys B187 is replaced by Leu in *E. coli* QFR, and Tyr B202 is replaced by Phe in *E. coli* and *W. succinogenes* QFRs and *E. coli* SQR. Therefore, *A. suum* QFR is more similar to mitochondrial porcine and chicken SQRs than bacterial complex II molecules with respect to the environment of the iron–sulfur centers.

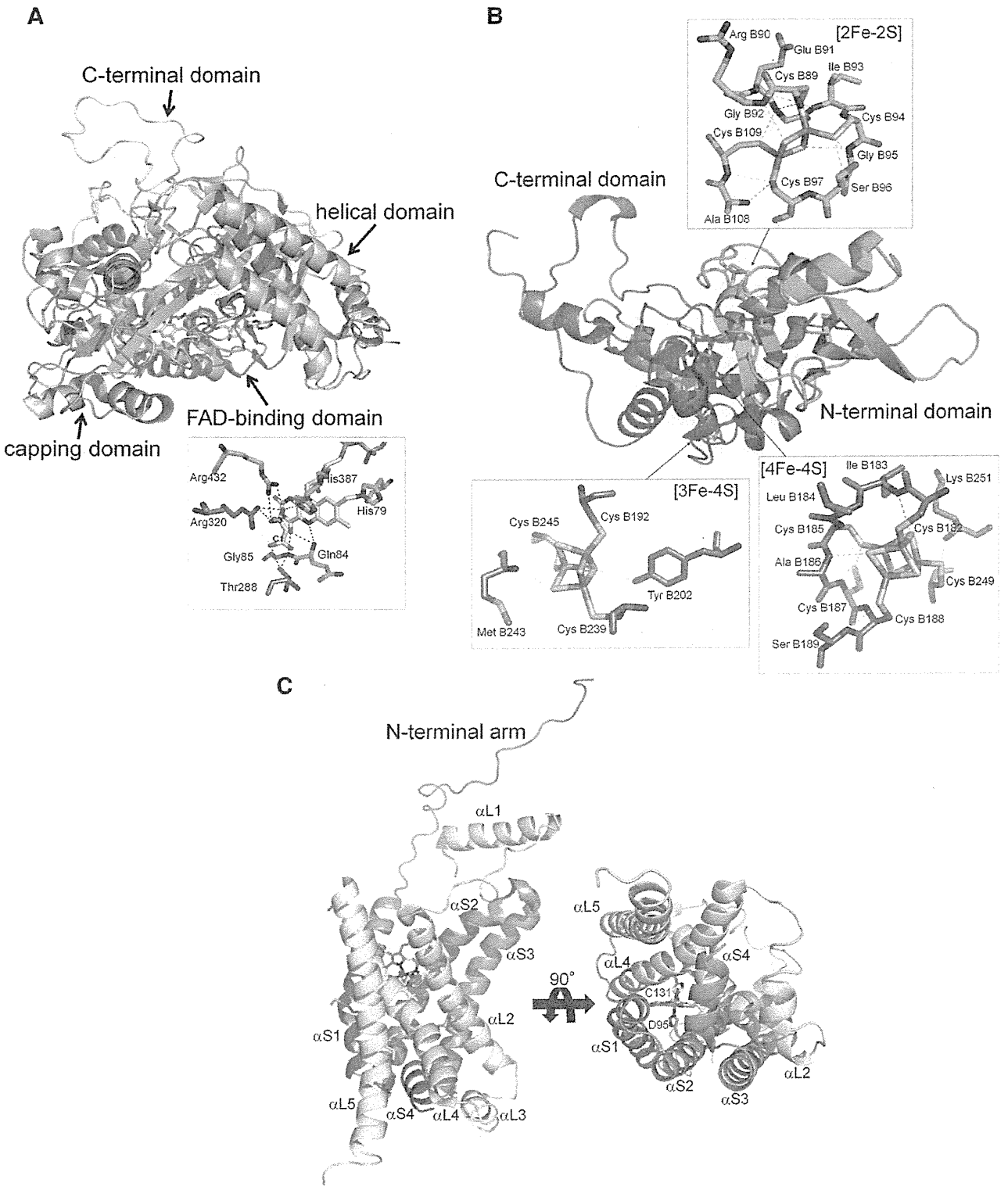

Fig. 4. Depiction of subunits. (A) Cartoon representation of the Fp subunit. The FAD-binding domain, capping domain, helical domain and C-terminal domain are shown in pale green, light blue, light pink and white, respectively, together with the stick models of FAD and malonate. The close-up view of the neighborhood of FAD is also represented in the inset. Color-coding for each atom type: C, white; N, blue; and O, red. Carbon atoms of residues from the FAD-binding domain and capping domain are shown in pale green and light blue, respectively. (B) Cartoon representation of the N-terminal domain (cyan) and C-terminal domain (light blue) of the Ip subunit together with the iron–sulfur centers shown as stick models. The close-up view of the iron–sulfur centers, cysteine ligands and residues interacting with the centers are shown in the insets. In (A) and (B), hydrogen bonds are shown with dashed lines. (C) Cartoon representation of the membrane-anchoring CybL (yellow) and CybS (orange) subunits together with heme *b* and the bound lipid molecule viewed from orientations perpendicular to each other. C131 and D95 are histidine residues from CybL and CybS subunits, respectively.

2.4. Transmembrane CybL and CybS subunits

The membrane anchor of *A. suum* QFR, like *E. coli*, porcine and chicken SQRs [21–23], is made up of CybL and CybS subunits. They are composed of five (CybL: αL1–αL5) and four (CybS: αS1–αS4) α-helices, of which αL2, αL4, αL5, αS1, αS2, and αS3 are transmembrane helices [20]. Four helices, αL2, αL4, αS1, and αS2, form a helix bundle in which a heme *b* molecule is accommodated through ligation of conserved His C131 and His D95 (Fig. 4C). Unlike the FAD molecule and the iron–sulfur centers, most residues near the heme *b* molecule are not conserved (Fig. 3C and D). A lipid molecule is bound below the heme *b* site in the helix bundle. Phosphatidylethanolamine is incorporated into the current model, although electron density patterns are not clear enough to identify the lipid species. Both heme *b* and lipid molecules are located at the interface of CybL and CybS subunits and may contribute to the assembly of the CybL and CybS subunits. Interestingly, a segment comprising 27N-terminal residues (D28–D54, Fig. 4C) of the CybS subunit extends to the Fp and Ip subunits and five residues (D29, D39, D41, D42, D46) form inter-subunit hydrogen bonds with residues of Fp (A471, A195, A192) and Ip (B150). The segment is unique to *A. suum* QFR, and seems to contribute to the stabilization of the multi-subunit structure of the enzyme. A definite cleft is formed at the interface of the Ip, CybL, and CybS subunits, and residual electron density probably revealing a bound RQ molecule is found in the cleft. The location of the cleft is in agreement with the quinone-binding sites assigned in the structures of other complex II molecules [18,21–23]. In the refined structure (3VR8), RQ is well situated in the cleft (Fig. 2) and is surrounded by residues that are highly conserved among complex II molecules from porcine, chicken and *A. suum* (Fig. 3C and D).

2.5. Mechanisms of fumarate reduction and rhodoquinol oxidization

The crystal structure of the fumarate-bound *A. suum* QFR (3VRB) clearly reveals that a fumarate molecule is bound to the dicarboxylate site in a non-planar conformation (Fig. 5A); C2, C3, and C4 carboxyl groups are in the same plane parallel to the FAD isoalloxazine ring but the C1 carboxyl group deviates from the plane as indicated by a C3–C2–C1–O1A dihedral angle of 83.7°. The non-planar conformation is stabilized by hydrogen bonds with conserved residues; the C1 carboxyl group with Gly A85, His A276, Thr A288, and Glu A289, and the C4 carboxyl group with Arg A320, His A387, Arg A432, and Ala A435. Accordingly, the structure suggests that the uniform distribution of π-electrons over the conjugated double bonds of fumarate is disrupted and that a partial charge separation, $C2^{\delta+}$ and $C3^{\delta-}$, is induced on the bound fumarate molecule. This charge separation seems to be the key to the reduction of fumarate because the contact of $C2^{\delta+}$ with FAD N5 (3.5 Å) observed in the crystal structure should facilitate the hydride (or hydride equivalent) transfer from reduced FAD N5 to $C2^{\delta+}$. The twisted conformation of fumarate is also observed in *E. coli* [29] and *W. succinogenes* [19] QFRs, as well as in flavoproteins such as flavocytochrome *c* [30] and *T. cruzi* dihydroorotate dehydrogenase [31], and the similar mechanism of fumarate reduction has been proposed for these enzymes. The crystal structure also suggests that conserved Arg A320 probably supplies a proton to $C3^{\delta-}$ to complete the fumarate reduction.

Fig. 5B shows the RQ binding site of *A. suum* QFR. Of 12 residues within 5 Å of the bound RQ, nine residues (B193, B194, B197, B240, B242, C72, C76, D106, and D107) are conserved in porcine, chicken, and *E. coli* SQRs (Fig. 3). The [3Fe–4S] center, the nearest iron–sulfur center to the bound RQ, is located at distances of 9.1 and 7.7 Å from RQ O1 and O2, respectively, indicating that electrons are transferred from RQH_2 to FAD *via* the [3Fe–4S], [4Fe–4S], and [2Fe–2S] centers. Although residues surrounding heme *b* are mostly not conserved among complex II molecules (Fig. 3), the possibility of heme *b* to act as an electron acceptor from RQH_2 remains because heme *b* is also the redox center close to the bound RQ (Fig. 2B) and its redox potential (−34 mV, [16]) is higher than that of RQH_2 (−63 mV). RQ is also surrounded by conserved amino acid residues in SQRs from porcine, chicken and *E. coli* (Ser C72, Arg C76, Asp D106, and Tyr D107) and is involved in these hydrogen bond networks: RQ O1····Tyr D107····Arg C76····Asp D106 and RQ O2····Ser C72····RQ N····Arg C76····Asp D106. Protons abstracted from RQH_2 can leave along these networks. It should be noted that the amino group of RQ, which is replaced by the methoxy group in ubiquinone, is involved in one of the hydrogen bond networks.

2.6. Flutolanil-binding site

In both crystal structures of *A. suum* QFR (Fig. 6A, 3VRB) and porcine SQR (Fig. 6B, 3AE8) complexed with flutolanil, an inhibitor specific for *A. suum* QFR [26], flutolanil is bound to the quinone-binding site located near the [3Fe–4S] center (Q_p site), where residues of *A. suum* QFR and porcine SQR within 5 Å of the bound flutolanil are mostly identical (73%). The isopropoxy-phenyl moiety of flutolanil comes in contact with conserved hydrophobic residues and the carbonyl oxygen forms hydrogen bonds with tyrosine and tryptophan residues. Accordingly, these hydrogen bonds as well as van der Waals contact seem to be important for the binding of flutolanil to both enzymes. It is worth noting that there is close contact between the isopropoxy group of the bound flutolanil and the aromatic indole ring of *A. suum* QFR Trp C69; these are separated by 3.3 Å, significantly less than the distance expected for van der Waals contact (3.7 Å), indicating that they interact with each other through a C–H····π interaction. Since the tryptophan residue is replaced by methionine (Met C39) in porcine SQR, this electrostatic interaction is unique to *A. suum* QFR. Another electrostatic interaction unique to *A. suum* QFR is formed between the flutolanil trifluoromethylbenzene moiety and Arg C76 guanidino group. Since the trifluoromethyl group is an electron-withdrawing group, the π-orbital of the flutolanil aromatic ring is expected to be deficient in electrons. In contrast, the π-orbital of the guanidino group of Arg C76 seems to be rich in electrons because the arginine residue located in the hydrophobic environment of the membrane-anchoring CybL subunit may preferentially the unprotonated form over the protonated one. Therefore, the stacking of the two π-orbitals, one is deficient and another rich in electron, with the distance of 3.2 Å observed in the *A. suum* QFR-flutolanil complex reinforce the attractive interaction between flutolanil and *A. suum* QFR. In porcine SQR, however, the guanidino group of Arg C46, the counterpart residue to Arg C76, is a greater distance from the flutolanil trifluoromethylbenzene moiety and is poorly stacked.

In contrast to flutolanil, 2-thenoyltrifluoroacetone (TTFA), a potent inhibitor against mammalian SQR, does not inhibit both *A. suum* QFR and SQR [11]. There are two TTFA binding sites in porcine SQR [22], Q_p and Q_d sites. The Q_p site TTFA, like flutolanil bound to the Q_p site, accepts hydrogen bonds and van der Waals contacts from residues that, except for Trp C35 (Pro C65 in *A. suum* enzymes), are conserved in the *A. suum* enzymes, whereas the Q_d site TTFA is surrounded mostly by residues unconserved in the *A. suum* enzymes and interacts with porcine SQR mainly through water molecules [22]. Therefore, if it is assumed that the Q_p site is more crucial for the inhibition of complex II than the Q_d site, the insensitivity of *A. suum* enzymes toward TTFA may be caused by the change from Trp C35 to Pro C65.

3. Twelve novel subunits of *T. cruzi* complex II

3.1. Subunit structure of T. cruzi complex II

The parasitic protist *T. cruzi* is the etiological agent of Chagas disease, a public health threat in Central and South America. These parasites are normally transmitted by the reduviid bug *via* vector feces after a bug bite and are also transferred *via* transfusion of infected

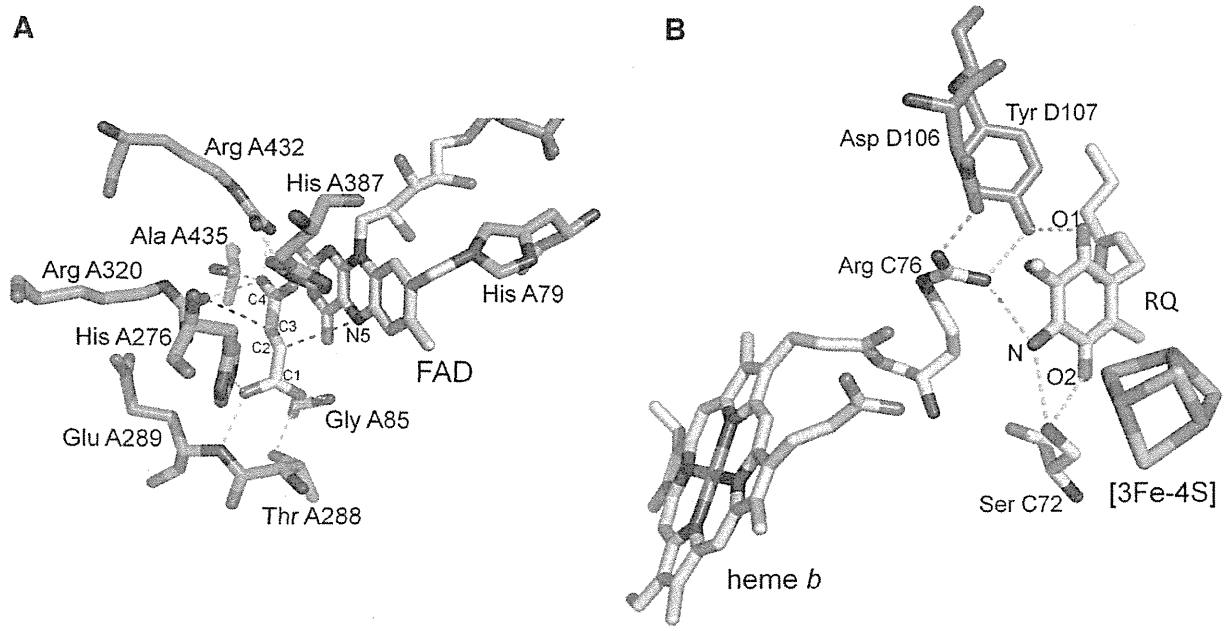

Fig. 5. Close-up view of active site structures. (A) The fumarate molecule bound to the dicarboxylate-binding site of *A. suum* QFR and residues interact with fumarate. Hydrogen bonds are shown in yellow dashed lines. Red dashed lines indicate probable routes of hydride (FAD N5→fumarate $C2^{\delta+}$) and proton (Arg A320 $N\eta \rightarrow C3^{\delta-}$) transfers to reduce fumarate. (B) Rhodoquinol binding site of *A. suum* QFR. Hydrogen bonds are shown in yellow dashed lines. Color-coding for each atom type is as follows: N, blue; O, red; S, dark yellow; and Fe, brown. Carbon atoms of FAD, RQ and heme *b* are shown in white, residues from Fp, CybL and CybS are shown in light green, yellow, and orange, respectively.

blood. About 16 to 18 million people are infected and 100 million are at risk, but there are no definitive chemotherapeutic treatments available [32].

To our surprise, the complex II purified from *T. cruzi* consists of six hydrophilic (SDH1, $SDH2_N$, $SDH2_C$, and SDH5–SDH7) and six hydrophobic (SDH3, SDH4, and SDH8–SDH11) nuclear-encoded subunits (Fig. 7; [24]). SDH1 and SDH2 correspond to Fp (SDHA) and Ip (SDHB), respectively. Orthologous genes for each subunit were identified in most trypanosomatids, including *T. brucei* and *Leishmania major* [33–35]. Notably, the iron–sulfur subunit was heterodimeric; $SDHB_N$ and $SDHB_C$ contain the plant-type ferredoxin domain in the N-terminal half and the bacterial ferredoxin domain in the C-terminal half, respectively. Catalytic subunits (SDHA, $SDHB_N$ *plus* $SDHB_C$, SDH3, and SDH4) contain all key residues for binding of dicarboxylates and quinones, but the enzyme showed lower affinity for both substrates and inhibitors than mammalian enzymes. In addition, the enzyme binds protoheme IX, but SDH3 lacks a histidine ligand [24].

3.2. Split Ip subunit of Trypanosomal complex II

In contrast to the monomeric iron–sulfur subunit (SDHB) found in all known families of complex II, the Trypanosomal iron–sulfur subunit is composed of two nuclear-encoded genes for $SDHB_N$ and $SDHB_C$ subunits (Fig. 7) [24]. The crystal structure of the Ip subunit from porcine complex II [22] and the PHYRE^2 model [36] of *T. cruzi* $SDHB_N$ (residues B_N66 to B_N161) and $SDHB_C$ (residues B_C34 to B_C163) are shown in Fig. 8A and B, respectively. The C-terminal extension of $TcSDHB_N$ (residues B_N162 to B_N270) was removed from the model to allow better comparison between porcine Ip (Fig. 8A) and split Trypanosomal Ip (Fig. 8B) subunits. According to this model, the [2Fe–2S] center is bound to the $TcSDHB_N$ subunit (Fig. 8B) by four cysteine residues, B_N120, B_N125, B_N128, and B_N140 (Fig. 9), which correspond to cysteine residues B65, B70, B73, and B85 from porcine SDHB [22]. The [4Fe–4S] center is bound to $TcSDHB_C$ by cysteine residues B_C71, B_C74, B_C77, and B_C138 (Fig. 9), which correspond to cysteine residues B158, B161, B164, and B225 from the porcine SDHB subunit and, finally, the [3Fe–4S] center is bound by cysteine residues B_C81, B_C128, and B_C134 (Fig. 9), which correspond to cysteine residues B168, B215, and B221 from porcine *SDHB* subunit [22]. The residues from SDHB subunit which interact with flutolanil from porcine complex II (B216, B218, B169, and B173 from Fig. 4B) are also found in $TcSDHB_C$ (B_C82, B_C86, B_C129, and B_C131 in Fig. 9). Thus, even if the Ip subunit of the Trypanosomatid complex II is comprised of two distinct peptides, the three iron–sulfur clusters as well as all cysteine residues necessary to bind those clusters are structurally conserved among all families of complex II. Such spatial organization of iron–sulfur clusters is expected to be crucial for optimal electron transfer from succinate to ubiquinone.

3.3. T. cruzi complex II as a drug target

Purified *T. cruzi* enzyme shows reduced binding affinities for both substrates and inhibitors. Its K_m values for ubiquinone (18.8 ± 6.4 μM (Q_2)) and succinate (1.48 ± 0.17 mM) were higher than those with bovine enzyme [37] (0.3 and 130 μM, respectively) and *E. coli* enzyme [38,13] (2 and 277 μM, respectively). Interestingly, the *T. cruzi* enzyme K_m value for succinate was comparable to 610 μM in adult *A. suum* [10], which expresses the stage-specific complex II as QFR under hypoxic environments in the host organisms mentioned above.

Sensitivity to inhibitors also differs from that of other complex II molecules. Atpenin A5, a potent inhibitor for complex II, inhibited the *T. cruzi* enzyme with an IC_{50} value of 6.4 ± 2.4 μM, which is three orders of magnitude higher than that of bovine enzyme (4 nM) [39]. Furthermore, *T. cruzi* enzyme does not respond to carboxin, 2-theonyltrifluoroacetone (TTFA), plumbagin, and 2-heptyl-4-hydroxyquinoline N-oxide (HQNO) (100 μM<IC_{50}). Structural divergence in Trypanosomatid SDH3 and SDH4 could be the cause for lower binding affinities for both quinones and inhibitors. In addition, the IC_{50} for malonate (40 μM) was much higher than the K_i value for bovine complex II (1.3 μM) [37], indicating different structures of the dicarboxylate-binding site.

These unusual features are unique in Trypanosomatidae and make their complex II molecules a target for new chemotherapeutic agents. Insensitivity to a known inhibitor is a promising feature for identifying a specific and potent inhibitor. Ascofuranone, which is a most

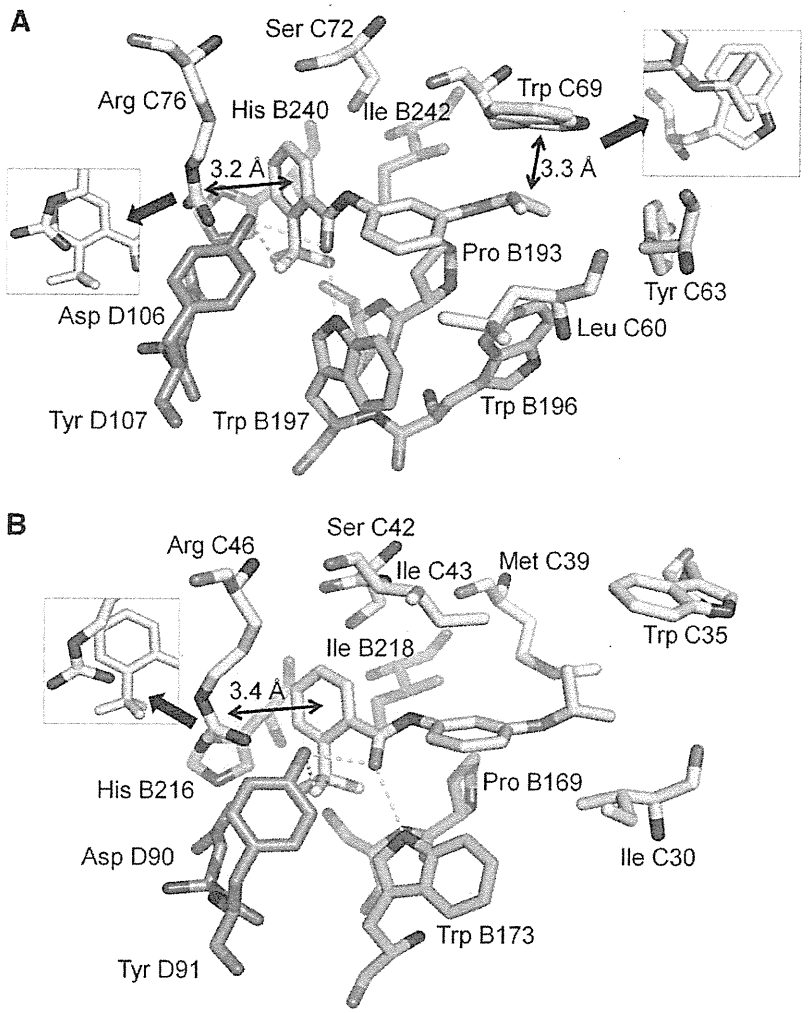

Fig. 6. Flutolanil binding site. The structures of flutolanil binding sites of (A) *A. suum* QFR and (B) porcine SQR. In each structure, the flutolanil molecule is bound to the quinone-binding site and surrounded by residues from Ip (cyan), CybL (yellow), and CybS (orange) subunits. Most of these residues are conserved between the two enzymes. Close-up views of the C—H·····π interaction between the isopropoxy group of flutolanil and Trp C69 side chain, and the electrostatic interaction between the flutolanil trifluoromethylbenzene moiety and Arg C76 guanidino group are shown in insets. Hydrogen bonds are shown in yellow dashed lines.

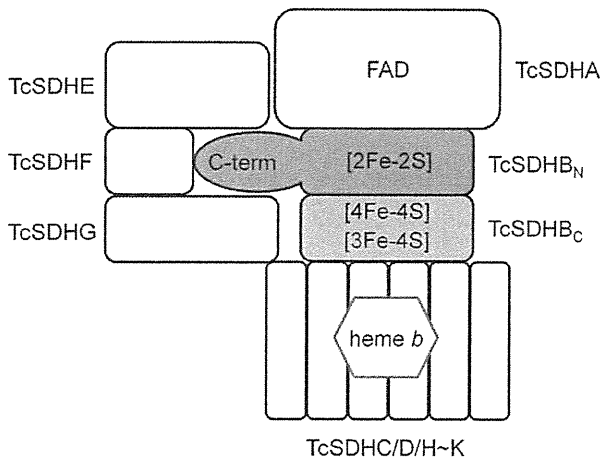

Fig. 7. Subunit organization model of Trypanosomal complex II. The Trypanosomal complex II is composed of six hydrophilic subunits (SDHA/B_N/B_C/E–G) and six hydrophobic subunits (SDHC/D/H–K). In the case of Trypanosomal complex II, the canonical SDHB is split into $SDHB_N$ (pink) and $SDHB_C$ (blue).

potent inhibitor of cyanide-insensitive alternative oxidase of *T. brucei* is good example [40].

4. Perspectives and conclusion

As described above, parasites have exploited a variety of energy-transducing systems in their adaptation to specific environments inside their hosts. Dynamic rearrangement of the respiratory chain during the life cycle is one of the key elements of this adaptation. However, the control mechanism responsible for stage-specific expression of the genes of parasites remains unclear because research on parasites at the molecular level has only recently begun. In this regard, recent reports indicating that complex II functions as an oxygen sensor are of great interest [41]. Mammalian cells are able to sense decreased oxygen availability and activate response systems, including transcriptional activation of several genes controlled via hypoxia-inducible factor-1 (HIF-1) [42]. Although the molecular mechanism of gene expression has not been elucidated for parasites, *A. suum* shows a very clear transition of the metabolic systems between larvae and adult stages, and it is, thus, a very promising research model. Our recent results show that a HIF-1 homologue plays a role in oxygen adaptation in *A. suum* and sequence analysis